DENSITY FUNCTIONAL THEORY INVESTIGATION OF RSNNSR SYSTEMS

By

Vadim V Nazarenko

Department of Chemistry
University of Louisville
Louisville, Kentucky

ACKNOWLEDGEMENTS

I am very grateful to my advisor, Dr. Mark E. Noble for his valuable help and guidance, enormous patience, and moral support throughout my studies. I also thank Dr. Pawel M. Kozlowski and Dr. Gene Lamm for helping me with my research and providing me with their valuable expertise. I extend my thanks to my friends and colleagues, Dr. Alexander V. Mayorov, Dr. Eduard Y. Chekmenev, Dr. Anton Petrov, Mr. James Quinn, Dr. Anton Rakitin, Mr. Chi Minh Tuong and Dr. Igor Vorobyov for their friendship and advice. I would also like to express my appreciation to my committee members, Dr. George R. Pack and Dr. Craig A. Grapperhaus for their most valuable comments and advice.

ABSTRACT

DENSITY FUNCTIONAL THEORY INVESTIGATION OF RSNNSR SYSTEMS

Vadim V Nazarenko

(Thesis director Dr. Mark E. Noble)

The structural variations and stabilities of RSNNSR systems were studied using the hybrid density functional theory (B3LYP) at various basis set levels. Computational methodology was based on the locally dense basis set approach (LDBS) that assigns various levels of the basis sets accordingly to the previously calibrated results that could be correlated to the experimental data.

The present study investigated the effect of the substituents (R) on the structure and the stabilities of RSNNSR systems. There were totally ten systems studied where R: H, CH_3, CF_3, *tert*-Butyl, C_6H_6, *p*-$NO_2C_6H_6$, *p*-$CH_3OC_6H_6$.

The calculations revealed that the stability of the S-N bond is enhanced if there is a combination of the electron-releasing effect and the electron-withdrawing one that creates a push-pull effect (captodative effect) in the system. An increase of a positive charge on one of the sulfur atoms and a negative charge on the adjacent nitrogen atom increases delocalization of one the S's lone pairs that creates a conjugation with the neighboring N atom and the β carbons through $2p\pi$-$3p\pi$ interactions.

The push-pull effect also influenced structural characteristics of the systems. One of the most notable ones is the variation of the NSCC dihedral angle in some of our systems from 89° to 21°

TABLE OF CONTENTS

PAGE

CHAPTER 1

INTRODUCTION

Thiodiazenes (diazosulfides) of the general formula R-S-N=N-R′ have been known for over one hundred years (1). Still, the literature on the subject is scarce (1-8). There are several areas in thiodiazene organic chemistry which have traditionally attracted the attention of researchers over the years, including photographic applications, as sources of diazenyl and thiyl radicals, dyes, and in synthetic applications (1,3,9-12). The relatively modest advances in thiodiazene chemistry are based on the fact that the S-N(=N) bond is very unstable. Thus, species with this bond are highly labile (13), although a number of thiodiazene systems have a relatively stable S-N=N lineage (14,15). In the mid-1970's, the interest in inorganic compounds with the S-N link was stimulated by the possibilities of sulfur – nitrogen chains as a potential new type of superconductive polymer (16). It was noticed that there is no predicted correlation between structural integrity of the systems and their molecular structure (9). Despite its long history there are still some unanswered questions about the S-N bond valency (17).

There is another, rather enormous research field in chemistry where S-N bonds play an important role. This field is located at the crossroads of inorganic, organometallic and biochemistry, namely, metal-sulfur chemistry (18,19). The interest in the metal-sulfur chemistry is promoted by the role that sulfur plays in various catalysts and enzymes.

All sulfur-metal catalysts can be grouped into three categories based on the particulars of their binding sites. The binding sites can be located on the metal centers or on the

sulfur atom, or the sites can involve both metal and sulfur atoms. The latter two are of the greatest interest to us.

There are several examples of sulfido catalysts where sulfur is a binding site of the catalysts (20-23). One area of research concentrates on the reactions between dihydrogen and activated sulfur. The Rakowski DuBois group reported dihydrogen homolytic addition to S_2^{2-} of a dinuclear Mo catalyst at ambient temperature and pressure (20,23). The essence of that research can be expressed by eq 1.1, where Cp′ stands for cyclopentadienyl or a substituted derivative.

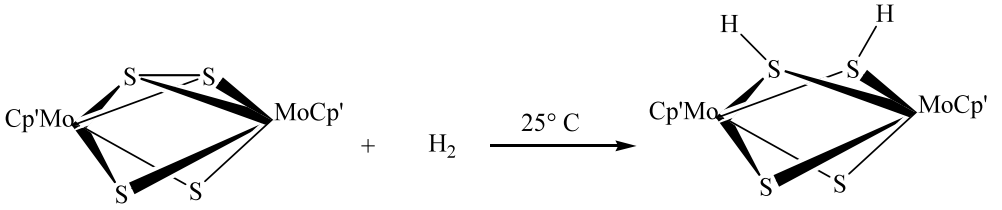

(1.1)

What is interesting about this reaction is that the product complex also has catalytic properties. Under mild reaction conditions (75° C and 1-2 atm of H_2), the bis(hydrosulfido) dimer can hydrogenate elemental sulfur to H_2S, activate ethylene and acetylene (eq 1.2 and 1.3), activate alkyl or aryl thiol (eq 1.4), and, participate in hydrodesulfurization (HDS) (eq 1.5).

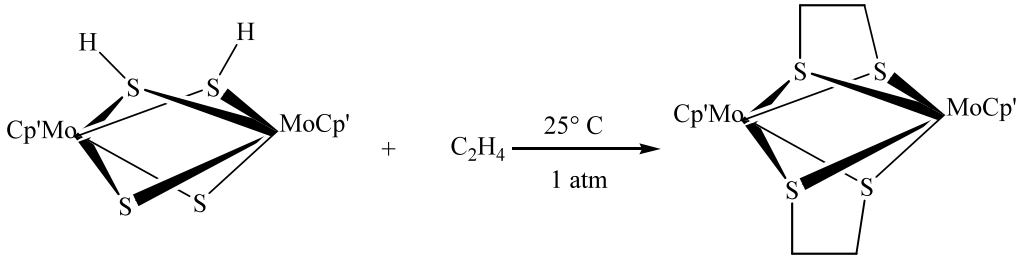

(1.2)

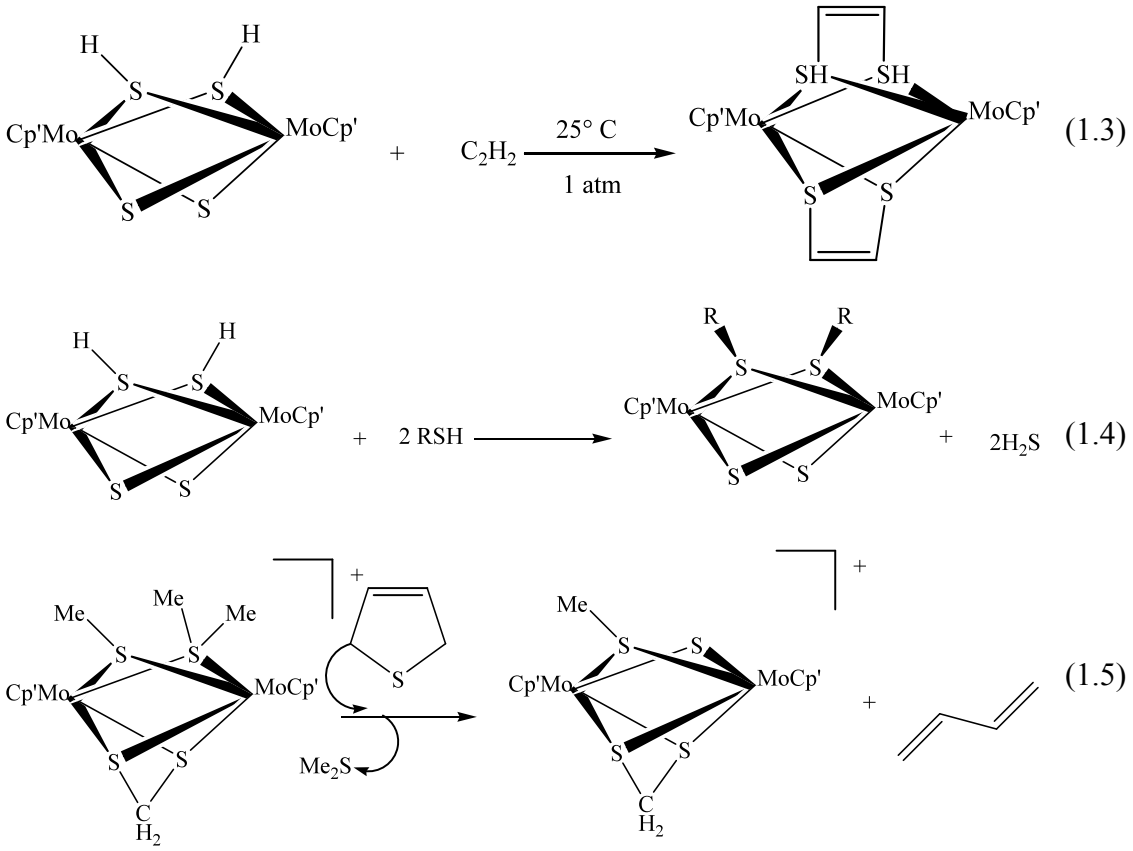

Besides studies that involved only sulfur as a catalyst active site, there were some studies that included sulfur and metal as a possible active site. One of the many examples of S-M active sites is the activation of acetylene and other alkynes. The binding modes could be summarized as in Figure 1.1.

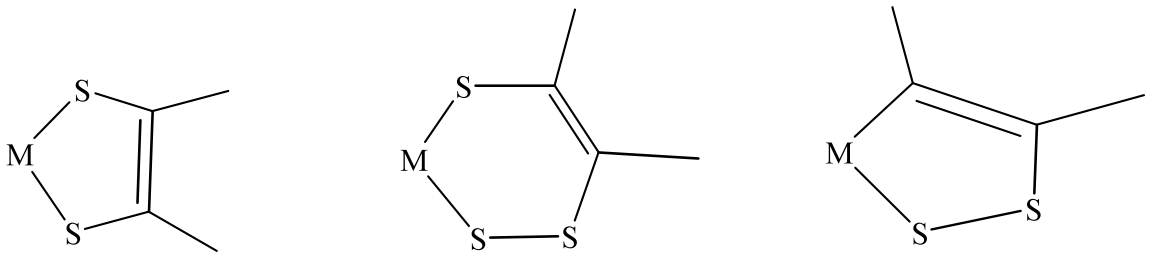

Figure 1.1. Possible binding modes of metal sulfur catalysts to alkynes.

One of these ways of coordination may be employed by nitrogenase to convert alkynes to olefins (24). The exact binding mode of the alkynes to nitrogenase is not yet understood. Also, the way dinitrogen binds to nitrogenase is not clear.

The importance of dinitrogen fixation cannot be overestimated. Diazotrophic bacteria can turn H_2O and N_2 into O_2 and NH_3 in mild conditions. The latter product is especially important for it is the primary source of nitrogen for plants' amino acids and therefore it is also important for animals. An alternative way to produce ammonia from N_2 and H_2 is the Haber-Bosch process. This process requires high temperature and high pressure. Thus, it is essential to understand nature's method of this process in the hope we can improve the industrial production of ammonia.

In nature, there are several bacteria that use nitrogenase enzymes. The enzymes consist of a complex of two metalloproteins, the homodimeric Fe-protein and the MoFe-protein. (V/Fe and Fe-only versions of the latter are also known but are much less common than the Mo/Fe protein.) The MoFe protein consists of two metal clusters: the P cluster that consists of Fe and S, and the MoFe-cofactor. It is presumed that reduction of dinitrogen occurs at the MoFe-cofactor through electron acceptance from the Fe protein and the P cluster (20-22).

Until recently it was thought that a solution to the problem of nitrogen fixation was within our reach (25,26). But, at this point in time, we are not even sure about the exact structural formula of the protein. The understanding of nature's process seems further away than previously thought (27). In the early 1990's there was a consensus that the Fe-Mo cofactor of nitrogenase had the structure shown in Figure 1.2.

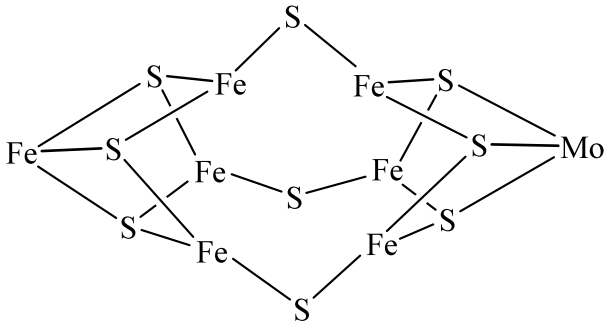

Figure 1.2. Proposed structure for the Fe-Mo cofactor prior to the 2002 (21).

The most recent study proposes a new structure for nitrogenase cofactor with an additional atom inside the cluster, shown in Figure 1.3.

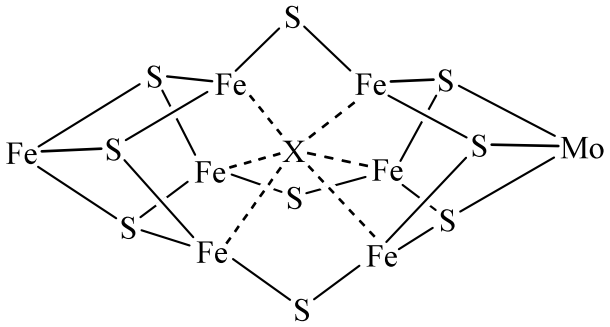

Figure 1.3. The most recent proposal for the structure of the Fe-Mo cofactor (22).

The identity of the atom 'X' is not known with certainty but it could be nitrogen, carbon, oxygen or sulfur (28). Also, the researchers are not sure if the atom 'X' is a part of the cofactor structure or if it is a byproduct of the natural enzymatic activity of the nitrogenase.

The way by which nitrogenase binds dinitrogen is not clear. Several approaches have been studied over the years. In light of the above-mentioned facts, it is possible that the metal-sulfur active sites might involve sulfur atoms during activation of a substrate as was noted above (29). Also, the presence of sulfur atoms in all types of nitrogenase

cofactors allows for sulfur-nitrogen bonds to be one possible step in the activation and/or reduction of dinitrogen at the active site. Some studies have postulated hydrogen bonding by the sulfur atom in the catalytic activity of the nitrogenase cofactor. This can be illustrated by Scheme I (30).

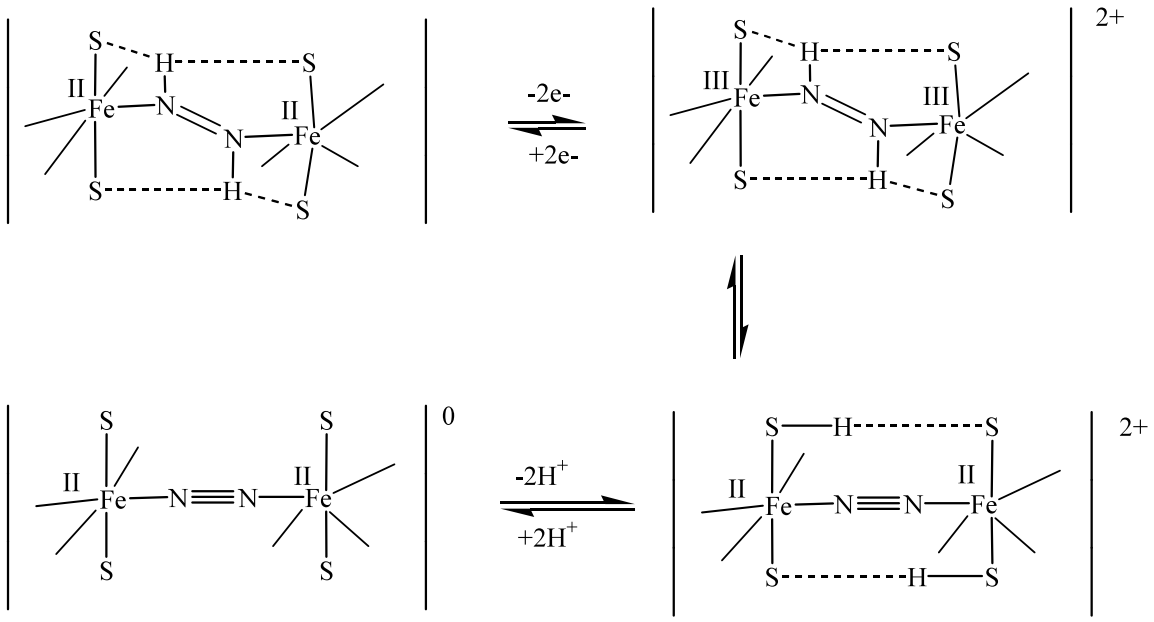

Scheme I

However, there remains the possibility for direct S-N covalency.

Our research group also made progress in synthesizing novel complexes of a sulfidomolybdenum dimer with sulfur as a binding site for substrate, for example, arenediazonium ion (1,6,8). The general reaction is represented by eq 1.6.

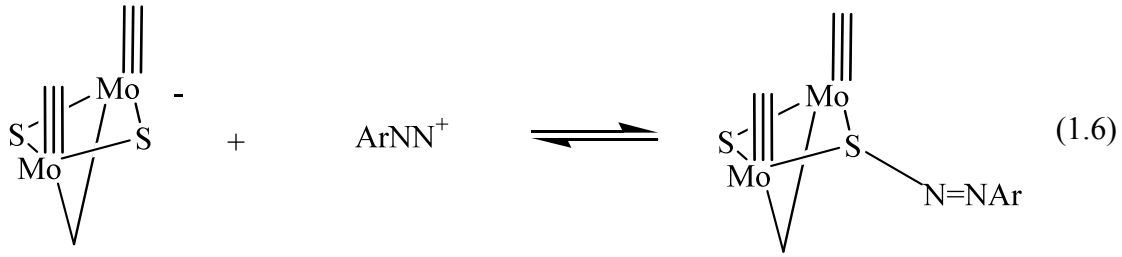

(1.6)

Besides, there were other compounds studied that were derivatives of the sulfidomolybdenum dimer (eq. 1.6), and that involved S-N bond, namely, the dimolybdenum thionitrites $Mo_2SN{=}O$ and the dimolybdenum sulfenimines $Mo_2SN{=}CH_2$, $Mo_2SN{=}CHR$, and $Mo_2SN{=}CR_2$ (6,8). The studies established that the substituents on the nitrogen atom influenced stability of S-N bond. The most stable were dimolybdenum sulfenimines, the least stable were the dimolybdenum thionitrites.

This notion introduces the need to study such covalent interactions. The present work involves computational studies of bis-thiodiazenes, RS-N=N-SR, as a study model for such interactions.

In the present research we investigated the impact of structural variations of the systems with the general formulae R-S-N=N-S-R on the covalency of the S-N bond and its energy. There were 14 systems studied. The study demonstrated the dependence of the S-N bond stability on the electronic environment of the substituents that were attached to the sulfur atom. The work reported here further advances our understanding of the S-N bond in the thiodiazene compounds and related systems.

CHAPTER 2

THEORETICAL BACKGROUND

2.1 INTRODUCTION

(Much of the material of this chapter is derived from references 24-31.)

An experiment that was performed by two American physicists, Clinton Davisson and Lester Germer, in 1925 demonstrated that particles have wave-like properties (25). Thus, it was established that matter has particle and wave character, which is termed wave-particle duality. In order to describe a position of a particle in space, we need to take into the consideration its wave-like character and to look at it as the amplitude of a wave. The wave in quantum mechanics that replaces the classical concept of trajectory is called a wave function and is denoted ψ.

In 1926, the Austrian physicist Erwin Schrödinger presented an equation for finding the wave function of any system (25,26). The general formula of the non-relativistic time-independent Schrödinger equation is

$$\hat{H}\psi = E\psi \tag{2.1}$$

where $\hat{H}$ is the Hamiltonian differential operator for a molecular system representing the total energy (25-27):

$$\hat{H} = -\frac{1}{2}\sum_{i=1}^{N}\nabla_i^2 - \frac{1}{2}\sum_{A=1}^{M}\frac{1}{M_A}\nabla_A^2 - \sum_{i=1}^{N}\sum_{A=1}^{M}\frac{Z_A}{r_{iA}} + \sum_{i=1}^{N}\sum_{j>i}^{N}\frac{1}{r_{ij}} + \sum_{A=1}^{M}\sum_{B>1}^{M}\frac{Z_A Z_B}{R_{AB}} \tag{2.2}$$

In the above equation, the first two terms describe the kinetic energy of the electrons and the nuclei. The third term represents the coulomb attraction between electrons and nuclei. The remaining two terms define the repulsion between electrons and nuclei.

The Schrödinger equation cannot be solved exactly for systems with more than two particles or for systems with distorted potential. The goal of quantum chemistry, therefore, is to find approximate solutions for the Schrödinger equation. We are going to discuss only approximation methods that are employed in the Hybrid Density Functional Theory methods.

2.2 BORN-OPPENHEIMER APPROXIMATION

The first approximation to the Schrödinger equation to consider is the Born-Oppenheimer approximation. This approach treats nuclear motions and electron motions separately; it regards the nuclei as fixed in position, solving the Schrödinger equation only for the electrons in the static electric potential arising from the nuclei. Hence, the complete Hamiltonian loses the second term, the kinetic energy of nuclei, and the last term, the repulsive interactions between nuclei, can be expressed as a constant.

A modified Hamiltonian or electronic Hamiltonian that describes the motion of electrons in the field of the stationary nuclei could be expressed as:

$$\hat{H}_{\text{elec}} = -\frac{1}{2}\sum_{i=1}^{N}\nabla_i^2 - \sum_{i=1}^{N}\sum_{A=1}^{M}\frac{Z_A}{r_{iA}} + \sum_{i=1}^{N}\sum_{j>i}^{N}\frac{1}{r_{ij}} \tag{2.3}$$

The solution to the Schrödinger equation with $\hat{H}_{\text{elec}}$ is then the electronic wave function, ψ_{elec}, and the electronic energy, E_{elec}. ψ_{elec} and E_{elec} depend on the electronic coordinates ($\boldsymbol{r}$, m_s) but do not explicitly depend on the nuclear coordinates, only parametrically ($\boldsymbol{R}$) (24).

The approximated Schrödinger equation, then, will have the form

$$\hat{H}_{\text{elec}}\,\psi_{\text{elec}}(\boldsymbol{r}, m_s; \boldsymbol{R}) = E_{elec}\,(\boldsymbol{R})\,\psi_{\text{elec}}(\boldsymbol{r}, m_s; \boldsymbol{R}) \tag{2.4}$$

The Born-Oppenheimer approximation uses the same approach to solve for nuclear motions. In this case, nuclei are considered as being in the electric potential arising from the electrons. A nuclear Hamiltonian is:

$$\hat{H}_{\text{nuc}} = -\frac{1}{2}\sum_{A=1}^{M}\frac{1}{2M_A}\nabla_A^2 \quad + E_{\text{tot}}\,(\{\mathrm{R_A}\}) \tag{2.5}$$

where

$$E_{\text{tot}} = E_{\text{elec}} + E_{\text{nuc}} = E_{\text{elec}} + \sum_{A=1}^{M}\sum_{B>A}^{M}\frac{Z_A Z_B}{R_{AB}} \tag{2.6}$$

$\{\mathrm{R_A}\}$ is an electronic Hamiltonian that serves as an electronic potential function for the internuclear motion.

From now on we will use mainly the electronic Schrödinger equation, eq 2.4.

2.3 VARIATIONAL APPROXIMATION METHOD

The variational method that uses Eckart's theorem (32) as its base was devised by J.W. Rayleigh. The variational method states that the energy, E^*, computed as the expectation value of a Hamiltonian, $\hat{H}$, from a trial normalized function, ψ^*, will always be higher than the true energy, E_0, of the ground state. Using bracket notation proposed by Paul Dirac (33), we could state that:

$$\langle \psi^* | \hat{H} | \psi^* \rangle = E^*(\alpha,\beta,\gamma...) \geq E_0 = \langle \psi_0 | \hat{H} | \psi_0 \rangle \tag{2.7}$$

where α, β, γ... are some arbitrary variational parameters. The expression, $E^*(\alpha, \beta, \gamma...) \geq E_0$, holds if and only if $\psi^* = \psi_0$.

Therefore, to find the ground state energy and ground state wave function, we need to minimize the expectation value of $\langle \psi^* | \hat{H} | \psi^* \rangle$ by manipulating the variational parameters

on which it depends. Saying this differently, we need to minimize the Rayleigh ratio, E^*, which is defined as

$$E^* = \frac{\langle \psi^* \left| \hat{H} \right| \psi^* \rangle}{\langle \psi^* \psi^* \rangle}$$

As we can see, we can minimize the functional $E[\psi]$ by searching through a certain set of wave functions (24,27).

The variational method is used for another approximation – the Hartree-Fock approximation method.

2.4 THE HARTREE-FOCK APPROXIMATION METHOD

The Hartree-Fock method includes a cluster of various approximations and methods including those that were mentioned above.

Historically, the Hartree-Fock approximation was started as D.R. Hartree's proposal to treat each electron of a physical system separately, representing each electron by a separate wave function, and with each electron occupying a separate orbital. An electron, then, would move in an average potential that is a product of all other electrons and the nuclei. Later, the approach was improved by V. Fock and J.C. Slater and it became known as the Hartree-Fock self-consistent field method or the Hartree-Fock method.

An orbital that is occupied by a single electron could be described by a wave function that includes space coordinates of the i-th electron, $\psi(\mathbf{r}_i)$, and one of two orthonormal spin functions, $\alpha(i)$ and $\beta(i)$, with spins + ½ and -½, respectively (24,25,31). A combined space-spin wave function is called a spin orbital and could be expressed as

$$\phi(i) = \psi(\mathbf{r}_i)\, \alpha(i) \qquad (2.8)$$

or

$$\phi(i) = \psi(\mathbf{r}_i)\ \beta(i) \tag{2.9}$$

A many-electron system Hamiltonian is a sum of one-electron Hamiltonians. Consequently, it makes a many-electron wave function, called a Hartree product, a product of single electron spin orbital wave functions (24).

$$\psi(1,2,\ldots,N) = \phi_a(1)\ \phi_b(2),\ldots,\phi_n(N) \tag{2.10}$$

The energy of a wave function of a multi-electron system, therefore, will be a sum of the single spin orbitals of the system.

$$E = \varepsilon_a + \varepsilon_b + \ldots + \varepsilon_n \tag{2.11}$$

A many-electron system that has paired electrons must take into account the Pauli exclusion principle: "The total wavefunction must be antisymmetric under the interchange of any pair of identical fermions and symmetrical under the interchange of any pair of identical bosons" (25). A fermion is an elementary particle that has half-integral spin, such as an electron. A boson is an elementary particle that has integer spin.

Taking into account the antisymmetric character of the many-electron system, we can express the ground state of such system as a secular determinant that consists of spin orbitals.

$$\psi_0(1,2,\ldots,N) \approx \psi(1,2,\ldots,N) = \frac{1}{\sqrt{N!}} \begin{vmatrix} \phi_a(1) & \phi_b(1) & \ldots & \phi_n(1) \\ \phi_a(2) & \phi_b(2) & \ldots & \phi_n(2) \\ \vdots & \vdots & \ldots & \vdots \\ \phi_a(N) & \phi_b(N) & \ldots & \phi_n(N) \end{vmatrix} \tag{2.12}$$

where $\phi_a, \phi_b,\ldots,\phi_n$ are spin orbitals with N number of electrons and $\frac{1}{\sqrt{N!}}$ is a normalization factor. The wave function $\psi(1,2,\ldots,N)$, given by eq 2.12, is called a determinantal wave function or, simply, a Slater determinant, paying a tribute to J.C.

Slater who first proposed to use it for quantum mechanical applications. The Slater determinant could be expressed by its shorthand notation, using its diagonal elements only, as

$$\psi(1,2,\ldots,N) = \frac{1}{\sqrt{N!}} \det \left| \phi_a(1)\ \phi_b(2)\ldots\phi_n(N) \right| \tag{2.13}$$

By swapping the places of two electrons of any electron pair, the sign of the determinant will change and that demonstrates its antisymmetric nature. Also, if two electrons occupy the same spin-orbital, the determinant will be equal to zero; that demonstrates that only one electron can occupy a spin orbital as a requirement of the Pauli exclusion principal. The exchange of two electrons with the same spin is correlated; that is called exchange correlation. Although the Slater determinant takes into account exchange correlation of two electrons with parallel spins, it neglects dynamic correlation of electrons with opposite spins. Because the motion of two electrons with opposite spins is not correlated, it is said that a single determinantal wave function is an uncorrelated wave function (24).

At this point we would like to recall the variational approximation method. Using the variation method we can find the spin orbitals that will give us the Slater determinant that yields the lowest energy. The individual spin orbitals are part of the Hartree-Fock equations, which are defined as

$$\hat{f}_i\ \phi_i(i) = \varepsilon_i \phi_i(i) \tag{2.14}$$

where $i = 1,2,\ldots, N$, ε_i is the orbital energy of the spin orbital, and $\hat{f}_i$ is an effective one-electron operator called the Fock operator:

$$\hat{f}_i = -\frac{1}{2}\nabla_i^2 - \sum_A^M \frac{Z_A}{r_{iA}} + \sum_u \left\{ \hat{J}_u(i) - \hat{K}_u(i) \right\} \qquad (2.15)$$

The first two terms represent a core Hamiltonian for electron *i*, i.e., the kinetic energy and the potential energy. The third term is the Hartree-Fock potential. *u* is a set of spin orbitals *a,b,...,n*. The Coulomb operator, $\hat{J}_u$, and an exchange operator, $\hat{K}_u$, are defined as follows:

$$\hat{J}_u(i)\ \phi_i(i) = \left\{ \int \phi_u^*(j) \left(\frac{e^2}{4\pi\varepsilon_0 r_{ij}} \right) \phi_u(j) dx_2 \right\} \phi_i(i) \qquad (2.16)$$

$$\hat{K}_u(i)\ \phi_i(i) = \left\{ \int \phi_u^*(j) \left(\frac{e^2}{4\pi\varepsilon_0 r_{ij}} \right) \phi_i(j) dx_2 \right\} \phi_u(i) \qquad (2.17)$$

The Coulomb operator represents the Coulombic interactions between electrons. Because these interactions are space related, the operator is called the local Coulomb operator. The exchange operator operates on spin orbitals of all points of space and is called a non-local operator.

Just as soon as we tackle the problem with spin-space correlations of the spin orbitals, we need to look at a situation where electrons of different spins are not combined in the same space or they are considered separately with different effective potentials for each electron. Such systems are called open-shell systems that have unrestricted HF approximation, as opposed to the systems with paired electrons or closed-shell systems with restricted HF approximation.

As seen above in eq 2.14, the Hartree-Fock equations are integro-differential equations and their spin orbitals are their eigenfunctions and their corresponding energies are eigenvalues. Having said that, we should notice that exact solutions for integro-

differential equations are possible only for spherically symmetric systems such as atoms. Also, we should notice that, because the Fock operator has a functional dependence on the solution of the spin orbital, the Hartree-Fock equations are not true linear eigenvalue equations; instead, these are nonlinear, pseudo-eigenvalue equations that should be solved iteratively. Once solved, the Fock operator becomes a Hermitian operator, which leads to spin orbitals with the lowest energy values. This, however, does not help us to solve spin orbitals of the non-spherical, non-symmetrical systems such as those of most molecules.

To resolve such a problem, Roothaan proposed to use a set of known spatial basis functions for describing a motion of a single electron that enables one to express molecular orbitals as a linear combination of atomic orbitals.

$$\psi_i = \sum_{\mu=1}^{K} c_{\mu i}\phi_\mu \tag{2.18}$$

Here, ϕ_μ is a set of the basis functions, and $c_{\mu i}$ are variational parameters or the expansion coefficients upon which a solution of a molecular orbital depends; K is the number of basis sets. We should notice that a spin variation is not a part of the variational parameters of the basis functions. Known spatial basis functions, i.e. spatial integro-differential equations that represent them, could be expressed as matrix equations. Therefore, by substituting eq 2.18 into eq 2.14 and, then simplifying, we have

$$\hat{f}(1)\sum_{\nu} c_{\nu i}\phi_\nu(1) = \varepsilon_i \sum_{\nu} c_{\nu i}\phi_\nu(1) \tag{2.19}$$

Multiplication of eq 2.19 by the complex conjugate function ϕ_μ^* on the left for a given μ, and then integrating it over all space will yield a matrix equation

$$\sum_{\nu} F_{\mu\nu} c_{\nu i} = \varepsilon_i \sum_{\nu} S_{\mu\nu} c_{\nu i} \qquad i = 1,2,3,\ldots,K \qquad (2.20)$$

where F_{μ} is the Fock matrix and S_{μ} is the overlap matrix. The Fock matrix is defined as

$$F_{\mu\nu} = \langle \phi_{\mu}^{*}(1) \left| \hat{f}(1) \right| \phi_{\nu}(1) \rangle \qquad (2.21)$$

The overlap matrix is defined as

$$S_{\mu} = \langle \phi_{\mu}^{*}(1) \phi_{\nu}(1) \rangle \qquad (2.22)$$

The solution to the determinant must be

$$\det \left| F_{\mu\nu} - \varepsilon_i S_{\mu\nu} \right| = 0 \qquad (2.23)$$

Eq 2.20 is a representative of a set of the Roothaan equations. Each equation represents one electron, i.e. one value of i. The whole set of equations could be represented as

$$Fc = Sc\varepsilon \qquad (2.24)$$

where c is a matrix of the expansion coefficients $c_{\mu i}$, and ε is a diagonal matrix of the orbital energies ε_i.

The Roothaan equations cannot be solved directly because the Fock matrix depends on the spatial wave function ψ_i. Therefore, by varying the coefficients, $c_{\mu i}$, and by expressing the operators and functions as matrices, the equations could be solved iteratively.

The Fock matrix, F_{μ}, could be represented in the terms of the Fock operator, $\hat{f}$,

$$F_{\nu\mu} = \langle \phi_{\mu}^{*}(1) \left| \hat{f}(1) \right| \phi_{\nu}(1) \rangle$$

$$= \langle \phi_{\mu}^{*}(1) \left| \hat{H}_{core}(1) \right| \phi_{\nu}(1) \rangle + \sum_{u}^{N/2} \left[\left\langle \phi_{\mu}^{*}(1) \left| \hat{J}_{u}(1) \right| \phi_{\nu}(1) \right\rangle - \left\langle \phi_{\mu}^{*}(1) \left| \hat{K}(1) \right| \phi_{\nu}(1) \right\rangle \right] \qquad (2.25)$$

In order to express the functions ϕ_i as matrices, we substitute a basis set function, ϕ_μ, for the spin orbital, ϕ_i,, in eq 2.16 and eq 2.17

$$\hat{J}_u(1)\,\phi_v(1) = \phi_v(1)\sum_{\lambda}\sum_{\sigma} c^*_{\lambda i} c_{\sigma i}\int \frac{\phi^*_\lambda(2)\phi_\sigma(2)}{r_{12}} dx_2 \tag{2.26}$$

By multiplying eq 2.26 by the complex conjugate function $\phi^*_\mu(1)$ and, then by integrating it, we have

$$\langle \phi^*_\mu(1) \left| \hat{J_u}(1) \right| \phi_\nu(1) \rangle = \sum_{\lambda=1}^{i}\sum_{\sigma=1}^{i} c^*_{\lambda i} c_{\sigma i} (\mu\nu|\lambda\sigma) \tag{2.27}$$

where $(\mu\nu|\lambda\sigma)$ is the two electron repulsion integral.

The exchange term could be expressed as

$$\langle \phi^*_\mu(1) \left| \hat{K_u}(1) \right| \phi_\nu(1) \rangle = \sum_{\lambda=1}^{i}\sum_{\sigma=1}^{i} c^*_{\lambda i} c_{\sigma i} (\mu\sigma|\lambda\nu) \tag{2.28}$$

where $(\mu\sigma|\lambda\nu)$ is the two electron exchange integral.

The Fock matrix (equation (2.25)) could be expressed as

$$F_{\lambda\mu} = \hat{\mathrm{H}}_{core} + \sum_{\lambda\sigma} P_{\lambda\sigma}\left[(\mu\nu|\lambda\sigma) - \frac{1}{2}(\mu\lambda|\sigma\nu)\right] \tag{2.29}$$

where $P_{\lambda\sigma}$ is a density matrix or a charge-density bond-order matrix, and can be defined as

$$P_{\lambda\sigma} = 2\sum_{i=1}^{N/2} c^*_{\lambda i} c_{\sigma i} \tag{2.30}$$

A density matrix is based upon the probability density distribution function, or the charge density, or the electron density

$$\rho(x) = 2\sum_{i}^{N/2} \phi^*_i(x)\phi_i(x) \tag{2.31}$$

Having the basic theoretical foundations of the Hartree-Fock self-consistent field method laid out, we can approach its procedural part.

First of all, the number, positions and identities of nuclei, the number of electrons of the molecule, and the basis set are assigned. Then, by assuming an initial set of orbitals, we can calculate an initial set of Fock operators. Having calculated the Fock operators, we can substitute them into eq 2.20 to compute a new set of orbitals, which concludes the first cycle of the SCF. The cycles will continue until there is no difference between two subsequent cycles. In reality, the difference between two cycles is almost never equal to zero but instead to an accepted threshold value. Iterations proceed self-consistently, and that explains the name of the procedure.

2.5 DENSITY FUNCTIONAL THEORY

The corner stone of density functional theory (DFT) is the electron density. An idea to express a system's total energy as a functional of the electron density was introduced by Thomas and Fermi, but it took a number of scientists (34,35) and dozens of years to make this theory available for practical purposes to computational chemistry.

The most important part of DFT that attracted scientists was its inexpensive calculations. We know that the wave function depends on 4N variables, where N is the number of electrons. Each electron has four variables, three spatial and one spin. In 1964, Hohenberg and Kohn came up with the first Hohenberg and Kohn theorem that states "the external potential $V_{ext}(\vec{r})$ is (to within a constant) a unique functional of $\rho(\vec{r})$; since, in turn, $V_{ext}(\vec{r})$ fixes $\hat{H}$, we see that the full many particle ground state is a unique functional of $\rho(\vec{r})$" (34,35). As the definition of this theorem shows, the electron density could uniquely determine the Hamiltonian and, therefore, the energy of the system. The

electron density is experimentally observed and depends on 8 variables, not 4N. Let us discuss DFT in more detail.

As we saw from the previous part of this Chapter, eq 2.31 permitted us to predict the probability to find an electron in a volume dx_i. Eq 2.31 could be expanded including not one but two electrons, giving us a possibility to calculate the pair density.

$$\rho_2(x_1,x_2) = \mathrm{N(N\text{-}1)} \int\ldots\int \left|\phi(x_1, x_2, ..., x_N)\right|^2 dx_3 \ldots dx_N \qquad (2.32)$$

The pair density, however, depends on the Coulombic forces and antisymmetric nature of the wave function that could be taken into an account by the reduced density matrix for one and two electrons (eq 2.33 and eq 2.34).

$$\rho_1(x,x') = N \int \psi\,(x,x_2,x_3,\ldots,r_N)\psi^*(x',x_2,x_3,\ldots,r_N)dx_2dx_3\ldots dx_N \qquad (2.33)$$

$$\rho_2(x_1,x_2,x_1',x_2') = \frac{N(N-1)}{2} \int \psi\,(x_1,x_2,x_3,\ldots,r_N)\psi^*(x_1',x_2',x_3,\ldots,r_N)dx_3\ldots dx_N \qquad (2.34)$$

We should notice that $x_1 = x_1'$ and therefore

$$\rho_2(x_1,x_1) = -\rho_2(x_1,x_1) \qquad (2.35)$$

Taking into account exchange-correlation effects (see eq 2.16 and eq 2.17) we have

$$\rho_2(x_1,x_2) = \rho(x_1)\,\rho(x_2)[1 + f(x_1; x_2)] \qquad (2.36)$$

where $f(x_1; x_2)$ is the correlation factor. The Fermi exchange and the Coulomb correlation produce the so-called exchange-correlation hole that is equal to the charge of one electron. The idea of the exchange-correlation hole is a theoretical basis for the exchange-correlation energy that could be defined as:

$$E_{XC}[\rho] = E_X[\rho] + E_C[\rho] \qquad (2.37)$$

It should be noted that exchange energy is the largest contributor to the overall exchange-correlation energy.

Going back to the first Hohenberg-Kohn theorem, we can express the ground-state electronic energy as:

$$E_0[\rho_0] = \int \rho_0 (x)\, V_{Ne} dx + T + V_{ee}[\rho_0] + E_{XC}[\rho_0] \tag{2.38}$$

where T represents kinetic energy.

Also,

$$E_0[\rho_0] = \int \rho_0 (x)\, V_{Ne} dx + F_{HK}[\rho_0] \tag{2.39}$$

where $F_{HK}[\rho_0]$ is the Hohenberg-Kohn functional which is a universal functional that is independent of external potential and is defined as

$$F_{HK}[\rho_0] = \left\langle \psi \left| \hat{T} + \hat{V}_{ee} \right| \psi \right\rangle \tag{2.40}$$

Therefore, we can say that there is direct correlation between the electronic density ρ of the ground state and the external potential V_{Ne}

$$E_0 = E_0^{V_{Ne}}[\rho_0] \tag{2.41}$$

The second Hohenberg-Kohn theorem laid the foundation for the variational principle in DFT. According to this theorem, the energy obtained from any trial density $\rho_t(x)$ which has the number of electrons (N) of the system as its functional, $\int \rho(x) dx = N$, is the upper bound to the true ground state energy.

$$E_0 \leq E^{V_{Ne}}[\rho_t] \tag{2.42}$$

The Hohenberg-Kohn theorems, however, do not specify functionals that should be used for solving DFT problems. In 1965, Kohn and Sham (KS) (35) developed a practical approach for the implementations of the Hohenberg-Kohn theorems.

The main idea of the KS approach is to express the kinetic energy T (see eq 2.37) of a system as a Slater determinant (eq 2.12) of the non-interactive, imaginary electrons. Therefore,

$$T = -\frac{1}{2}\sum_{i}^{N}\left\langle \varphi_i \middle| \nabla^2 \middle| \varphi_i \right\rangle \tag{2.43}$$

where φ_i is a spin orbital, called a Kohn-Sham orbital. In parallel to eq 2.14, we have

$$\hat{f}^{\,\mathrm{KS}}\varphi_i = \varepsilon_i \varphi_i \tag{2.44}$$

where the Kohn-Sham operator $\hat{f}^{\,\mathrm{KS}}$ is defined as

$$\hat{f}^{\,\mathrm{KS}} = -\frac{1}{2}\nabla^2 + V_{lp} \tag{2.45}$$

where V_{lp} is local potential. As we can see, eq 2.44 represents a single-particle equation that includes density of the system.

Despite the fact that we are not using real electrons still, we obtain the real electron density

$$\rho(x) = \sum_{i=1}^{N}\left|\varphi_i(x)\right|^2 \tag{2.45}$$

This electron density could be used for the calculations of the exchange-correlation energy that is a centerpiece of the Kohn-Sham approximation method, which is expressed as

$$E_{XC}^{LDA}[\rho] = -\int dx \frac{3}{4}\left(\frac{3}{\pi}\right)^{\frac{1}{3}}\rho^{\frac{4}{3}} \tag{2.46}$$

where LDA stands for the approximation of the exchange energy that in DFT is called the local density approximation (LDA). The name LDA is derived from the fact that the

exchange energy, which by nature is non-local, depends on the local values of the electronic density as shown in eq 2.46.

The exchange potential is

$$V_X^{LDA}(x) = -\left(\frac{3}{\pi}\rho(x)\right)^{\frac{1}{3}} \tag{2.47}$$

The total exchange-correlation energy could be expressed as

$$E_{XC}^{LDA} = \int \varepsilon_{XC}^{LDA}[\rho(x)]\rho(x)dx \tag{2.48}$$

where ε_{XC}^{LDA} is the exchange-correlation energy distribution per unit volume of the electronic density with local dependency.

If we go beyond LDA's dependence on electronic density $\rho(x)$, but substitute it for electronic spin densities $\rho_\alpha(x)$ and $\rho_\beta(x)$ that are composite parts of $\rho(x)$

$$\rho(x) = \rho_\alpha(x) + \rho_\beta(x) \tag{2.49}$$

then we have the local spin-density approximation (LSD) whose energy could be expressed as

$$E_{XC}^{LSD} = \int \varepsilon_{XC}^{LSD}[\rho_\alpha(x), \rho_\beta(x)]\rho(x)dx \tag{2.50}$$

Accounting for non-homogeneity of an electron density made significant improvement for the computations of the exchange-correlation energy. This was done by introducing the generalized gradient approximations (GGA) that uses the generalized gradient of the charge density, $\nabla\rho(x)$. Therefore,

$$E_{XC}^{GGA} = \int f(\rho_\alpha, \rho_\beta, \nabla\rho_\alpha, \nabla\rho_\beta)dx \tag{2.51}$$

and also

$$E_{XC}^{GGA} = E_X^{GGA} + E_C^{GGA} \tag{2.52}$$

The exchange part of the exchange-correlation energy could be expressed as:

$$E_X^{GGA} = E_X^{LDA} - \sum_\sigma \int F(s_\sigma)\rho_\sigma^{4/3}(x)dx \tag{2.53}$$

where s_σ is the reduced density gradient for spin σ (local inhomogeneity parameter)

$$s_\sigma(x) = \frac{|\nabla\rho_\sigma(x)|}{\rho_\sigma^{4/3}(x)} \tag{2.54}$$

In 1988, Becke further improved the GGA by introducing the gradient-corrected exchange functional

$$E_X^{Becke88} = E_X^{LDA} - \frac{\beta s_\sigma^2}{1 + 6\beta s_\sigma \sinh^{-1} s_\sigma} \tag{2.55}$$

where β is experimentally determined exchange energies of inert gases that is equal to 0.0042 Hartrees (36).

For the gradient-correlated correlation functionals, we should mention two of them, namely those of Perdew and Wang, 1991 (PW91) (55-58) and Lee, Yang and Parr, 1988 (LYP) (41,42).

According to PW91, the local part of the correlation energy is

$$E_C^{PW91}[\rho] = \int \rho E_C^{LDA}(r_s, \zeta)\, dx \tag{2.56}$$

where

$$r_s = \left[\frac{3}{4\pi\rho}\right]^{1/3} \tag{2.57}$$

and

$$\zeta = \frac{\rho_\alpha - \rho_\beta}{\rho_\alpha + \rho_\beta} \tag{2.58}$$

LYP is another gradient-corrected correlation functional. LYP is not based on E_C^{LDA} and uses parameters that were derived for the correlation energy of the helium atom. It includes one empirical parameter and some local components. We should note that the correlation functionals described here, PW91 and LYP, concentrate primarily on the dynamic or short-range correlation effects.

In 1993, Becke proposed DFT/HF hybrid functionals by a combination of the density functionals for exchange and exact Hartree-Fock exchange (61). The hybrid DFT that uses three empirically obtained parameters could be used in conjunction with LYP or PW91 correlation functionals. The values of Becke's three parameters were based on 56 atomization energies, 42 ionization potentials, 8 proton affinities, and second-period elements' atomic energies (43). The B3LYP exchange-correlation energy expression is

$$E_{XC}^{B3LYP} = (1-\mathrm{a})\,E_X^{LSD} + aE_{XC}^{\lambda=0} + bE_X^{B88} + cE_C^{LYP} + (1-c)E_C^{LSD} \qquad (2.59)$$

where a=0.20, b=0.72, and c=0.81. The λ=0 limit represents the exchange contribution of a Slater determinant.

Because of the contribution from HF, hybrid DFT could be solved iteratively employing SCF as was described above.

2.6 BASIS SETS

As mentioned above in Section 2.3 of this chapter, Roothaan proposed to use a set of known spatial basis functions for describing the motion of a single electron that enable one to express molecular orbitals as a linear combination of atomic orbitals (LCAO). The sum of the atomic orbitals (eq 2.18) forms the basis set. There are several types of basis sets available today.

One of them, STO-*N*G basis set, is a combination of two types of basis functions STO (Slater-type orbitals) and GTO (Gaussian-type orbitals, (44)).

The Slater-type functions have the form

$$\psi_{nlm_l}(\zeta,r\text{-}R_A) = N r^{n_{eff}-1} e^{-\zeta|r-R_A|} \tag{2.60}$$

where N is a normalization constant and $-\zeta$ is the Slater orbital exponent.

The Gaussian-type orbitals have the form

$$\psi_{ilk}(r_l - R_c) = (x_l - x_c)^i (y_l - y_c)^j (z_l - z_c)^k \; e^{-\alpha|r_l - R_c|^2} \tag{2.61}$$

where (x_c,y_c,z_c) (x_l,y_l,z_l) are the Cartesian coordinates of the center of the Gaussian at R_c and the Cartesian coordinates of an electron at r_l, respectively; $-\alpha$ is the Gaussian orbital exponent.

In order to achieve higher accuracy in calculations, several Gaussian functions (also called primitive Gaussian functions) are linearly combined together to produce a contracted Gaussian function (CGF), χ, of the form

$$\chi_j = \sum_i d_{ji} g_i \tag{2.62}$$

where d_{ji} are the contraction coefficients and g is the primitive Gaussian function with i parameters.

The simplest basis set is that with one function representing one orbital. A minimal STO-3G basis set would include linear combination (contraction) of three primitive Gaussian functions. Substituting each of the minimal basis functions with two basis functions will improve the STO-*N*G basis set. The name for this new, improved type of basis sets is double-zeta basis set (DZ). Consequently, if we use three basis functions in place of one minimal basis function, we then have a triple-zeta basis set (TZ). A

compromise between computational demands of DZ and TZ resulted in a split-valence basis set (SV). SV basis sets would represent each core shell atomic orbital with a single basis function and each valence atomic orbital with two basis functions.

One of the examples of the SV basis sets is the 3-21G (45-51) basis set that includes one function with three primitives for the inner shell and two functions for each valence shell orbital, a contracted Gaussian of two primitives and a single primitive.

In order to compensate for atomic orbital distortions when the value of the quantum number is larger than classically accepted, some polarization functions of *p, d, f,* and *g* type are added. These can be denoted as 6-31G* or 6-31G(d). Also, some corrections are needed for systems with diffused electronic clouds, such as ions. In this case, diffuse functions are added to the basis sets (6-31G*(+)).

CHAPTER 3

STRUCTURAL STUDIES OF RSN=NSR TYPE SYSTEMS USING HYBRID DENSITY FUNCTIONAL THEORY

3.1 INTRODUCTION

Structural studies of thiodiazenes have been attracting the attention of chemists for quite some time (2,5,6). All studies have concentrated on the monosubstituted thiodiazenes, RSN=NR. In this work we directed our investigation to the bis-thiodiazenes of the general formula RSN=NSR. Such species were reported as possible intermediates ([PhSN=NSPh]) in the trisulphenamide decomposition reaction (52,53), but there were no follow up studies done.

Also, it is interesting to compare the structural specifics of bis-thiodiazenes to the geometries of their oxygen analogs, hyponitrous acid and *trans*-di-*tert*-butyl hyponitrite that were studied previously (11,54).

3.2 COMPUTATIONAL METHODS

The calculations were performed using Gaussian 98 revision A.7 software suite (55).

For the calculations, we employed Hybrid Density Functional Theory (HDFT) -- B3LYP method with Becke's three-parameter non-local exchange and Lee-Yang-Parr's non-local correlation functionals (36,41-43,56,57).

There were fourteen systems studied (see following page).

There were several basis sets (see Section 2.6 for details) used in the course of the calculations.

(*Z*)-bis(hydrosulfido)diazene

1

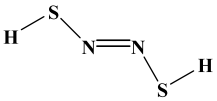

(*E*)bis(hydrosulfido)diazene

2

cis-hyponitrous acid

3

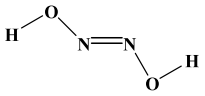

trans-hyponitrous acid

4

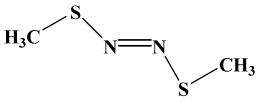

(*E*)-bis(methylthiolate)diazene

5

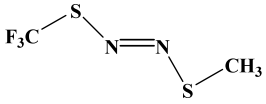

(*E*)-1-trifluoromethylthiolate-2-methylthiolatediazene

6

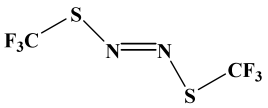

(*E*)-bis(trifluoromethylthiolate) diazene

7

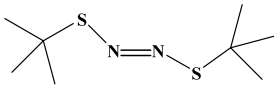

(*E*)-bis(*tert*-butylthiolate) diazene

8

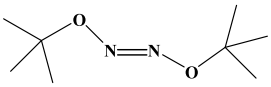

trans-di-*tert*-butyl hyponitrite

9

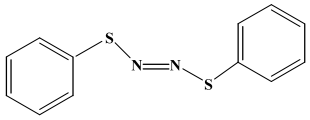

(*E*)-bis(phenylthiolate)diazene

10

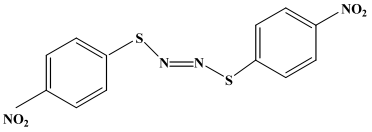

(*E*)-bis(4-nitrophenylthiolate)diazene

11

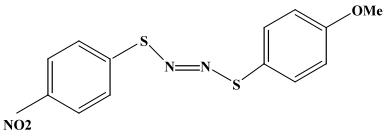

(*E*)-4-nitrophenylthiolate-4′-methoxyphenylthiolatediazene

12

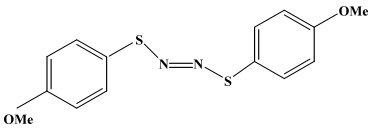

(*E*)-bis(4-methoxyphenylthiolate)diazene

13

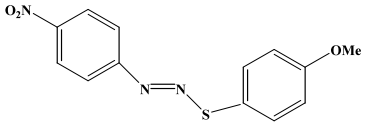

(*E*)-4-nitrobenzenediazo-4′- methoxythiophenolate

14

For the initial step we used only STO-3G basis set (58,59), with three primitive Gaussians. Subsequent steps involved Pople-type basis sets: split valence shell double-zeta plus polarization 3-21G* basis set, split valence shell double-zeta plus double polarization 6-31G(*, *) basis set, and split valence shell triple-zeta plus double polarization 6-311G(*, *) basis set. Polarization and diffusion functions of 6-31G and 6-311G basis sets have been adjusted according to the computational needs. The search for the global minima of the potentials was verified by screening the frequency calculations of the systems for imaginary frequencies.

During our calculations, we encountered several difficulties in obtaining convergence for structures 8 through 14. The cause of the problem is rooted in the fact that the molecules have flat potentials. Force constants that are produced by the initial guess for the second derivative matrix from a valence force field can differ considerably from the true values. In order to improve calculations, the Gaussian manual (60) suggests computing the force constants during the initial step using higher theory level or computing the force constants at every point of the optimization (keywords: Opt=CalcFc, Opt=CalcAll). The second way to deal with the flat potentials of large systems is to utilize GDIIS (61) (Geometry based on Pulay's Direct Inversion in the Interactive Subspace extrapolation method). In our case, the ways proposed by Gaussian to improve the calculations did not yield satisfactory results. Another way proposed by Gaussian for certain situations was not to vary the accuracy of the integrals during the initial SCF cycles (keyword: scf=novaracc). This approach also produced minimal success. Although none of these approaches worked for us, a combination of GDIIS method and the more

accurate calculations of the integrals at the initial SCF cycles – "no vary accuracy", produced excellent results.

3.3 COMPUTATIONAL EVALUATION OF (*E*)-4-NITROBENZENEDIAZO-4′-METHOXYTHIOPHENOLATE, **14**

A computational investigation, regardless of its accuracy, needs experimentally obtained values for validation. In our case, the experimental database is virtually nonexistent due to that fact that no bis-thiolatediazene compound has ever been isolated. Therefore, we tried to find a group of compounds that chemically and/or electronically were as close to the systems of interest (**1**-**2**, **4**-**8**, **10**-**13**) as possible, and that had experimental structural parameters available. Compounds that were chosen to be the models for the computational evaluation are **3**, **4**, **9** and **14**.

Because compound **14** is chemically and electronically relatively close to some of our systems (**10**-**13**), and at the same time it is as computationally challenging as the systems of interest (all have flat potentials and the third row element sulfur), we chose to investigate it first. Having said that, we would like to note that we decided to investigate the *E* conformer of **14** because there was experimental data for it.

The geometry optimization of **14** was performed in several steps. Initial geometry optimization of the system was used as a basis for the next calculation and the second geometry optimization was used as a basis for the third computation and so on. For the first step, one of the simplest basis sets STO-3G was employed (for the basis set descriptions see Chapter 2) (58,62). Then, the following steps utilized 3-21G* (46,48-51,63), 6-31G(d, p) (64-69), and 6-311G(d,p) basis sets (70-74). The final stage of the geometry optimization of **14** involved a complex basis set approach that became known

in the related literature as “the splicing” (75) or locally dense basis sets method (LDBS) (75-79). The essence of LDBS is to assign different basis sets to different atomic centers of a molecule.

Systematic applications of LDBS began to be developed in the 1970s and early 1980s (63,69,71,72). Huber and Diel employed LDBS for the calculations of the electric field gradients (80). Chesnut and Moore developed a LDBS method for NMR related calculations (81). In 1990, Jensen and Gordon applied LDBS for calculations of molecular geometries, Mulliken charges, and internal rotational barriers (75).

The systems that Jensen and Gordon studied were $CH_3CH_2CH_2OH$ and $CH_3CH_2XH_n$, where XH_n=F, OH, NH_2, CH_3. They reached the conclusion that, for geometry optimization, LDBS works the best across homonuclear or homoelectronegative bonds, such as C-C bonds. Also, they pointed out that they preferred to assign extended basis sets to “the chemically interesting part of the molecule” (75), while treating the rest of the molecule with lower levels of theory.

In our approach to investigate **14** we decided to assign a region of primary interest to the S-N=N part of the molecule (76-79). Reasons for this were that this region represents the weakest link of the molecule, the S-N bond is susceptible to a facile decomposition, and the S-N=N link is the primary object of our studies (1,3-5,9).

Our final, pre-LDBS step utilized the split valence shell triple-zeta plus double polarization 6-311G(d, p) basis set that uses three sizes of contracted functions with one d and one p polarization functions for the first three rows of atoms. The results, along with selected structural parameters and experimental values of **14,** are provided in Table 3.1. Results in Column 1 demonstrate that an absence of the diffuse functions on S, N_1, and

N_2 failed to correctly represent crucial bond lengths of N-S and S-C. (For details on this section, see Appendix 1). An assignment of the diffuse functions to all atomic centers except hydrogen brought bond distances closer to experimental values. Column 2 shows results of the calculations which used basis sets with one diffuse function added to all heavy atoms. Column 3 has two diffuse functions added to the heavy atoms. Columns 4, 5 and 6 demonstrate results of the calculations with one or two diffuse functions on the heavy atoms (Appendix 1, Figure A1.14). The results in the column 4 are based on the calculations that involved an assignment of two diffuse functions to S, O and N's of the nitro group; one diffuse function was assign to the remaining nitrogen atoms. In the column 5 two diffuse functions were placed on S atom and two nitrogen atoms of the diazo group, one diffuse function – on the remaining nitrogen atoms, all O and C atoms. In the column 6 this distribution was as follows: two diffuse functions on all O atoms, N atoms of the nitro group and S, one diffuse function on the remaining N atoms and C that is bonded to S.

The results of the calculations of the bond lengths in the Columns 4, 5 and 6 are in excellent agreement with the experimental values with one exception (Figure 3.1). This demonstrates that it is crucial to find the proper distribution of the diffused functions of the atomic centers about the molecule. The best results were obtained when two diffused functions were assigned to S; one diffused function was assigned to N_1, N_2 and C_8. We used these conclusions for the computational studies of **10**-**13**.

The exception to the good results obtained above was a divergence of 10° in the evaluation of the dihedral angle $N_1S_{31}C_8C_3$ of **14**. This may be explained by the fact that we investigated our systems in the gas-phase, but the experimental data was obtained

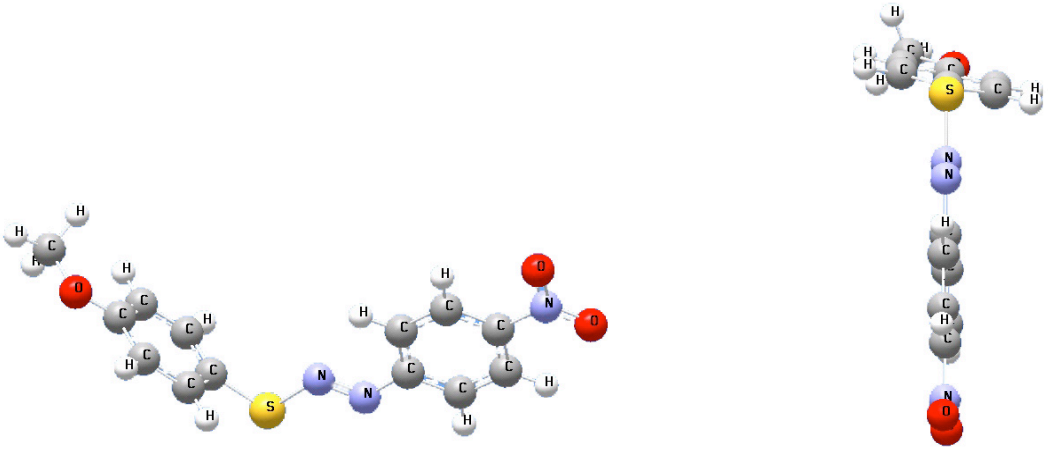

Figure 3.1 Final structural results of the geometry optimization of **14**.

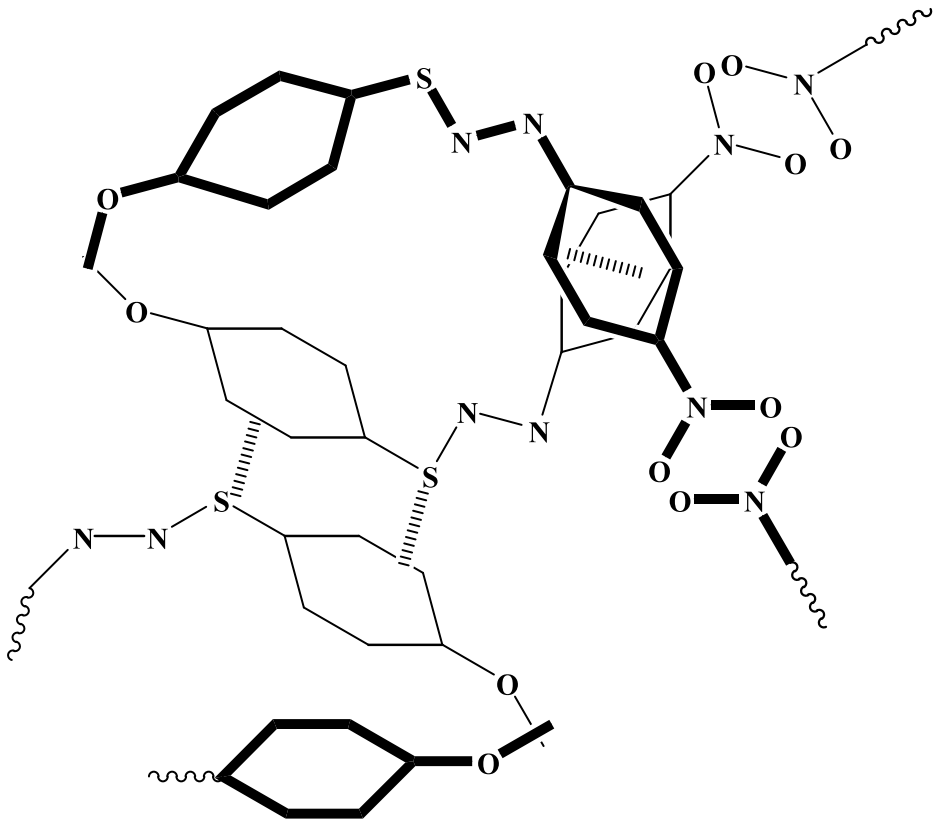

Figure 3.2. A unit cell of the crystal lattice of **14** (2). The molecules with bold lines are closer to the viewer. Hashed lines indicate possible intermolecular interactions.

from a crystal structure. Therefore, dihedral distortions of the crystal structure could be caused by the intermolecular interactions of **14** as it shown in Figure 3.2 (2). One kind of interaction is between lone pairs of sulfur atoms and the aryl group of the methoxythiophenolate; the second interaction is between nitrophenyl groups.

3.4 COMPUTATIONAL EVALUATION OF THE STRUCTURES OF **10 - 13**

Computational results for the geometry optimization of **10 - 13** are reported in Table 3.2.

The results of the calculations are consistent with the structural trends of compound **14**. The most significant differences that could be found among compounds **10 - 13** (Figures 3.3 - 3.6) reside in their S-N bonds and in their NSCC dihedral angles. The greatest difference in the S-N bond length is between structures **11** and **13**, 0.035Å. The most noticeable difference in dihedral angles is between structures **13** and **12**.

A Natural Localized Molecular Orbital (NLMO) analysis, which is part of the NBO 4.0 software package (82), helped us to understand structural variations of **10**, **11**, **12** and **13**. The NLMO analysis shows that the principal difference among systems **10** through **13** is in the degree of delocalization of one of the lone pairs of sulfur atoms.

The lone pair delocalization has a π-bonding character that is a result of the interaction of sulfur's 3p orbital with 2p orbitals of the neighboring atoms and/or with π-orbitals of the aryl ring (83). This delocalization accounts for 10% - 12% of the electronic density one of sulfur's lone pair to the neighboring atoms (Table 3.3). The most crucial direction of the electron delocalization that influences the dihedral angle ϕNSCC is a donation of the electron density to the aryl group. Dihedral angles of **11** and **12** are closest to the

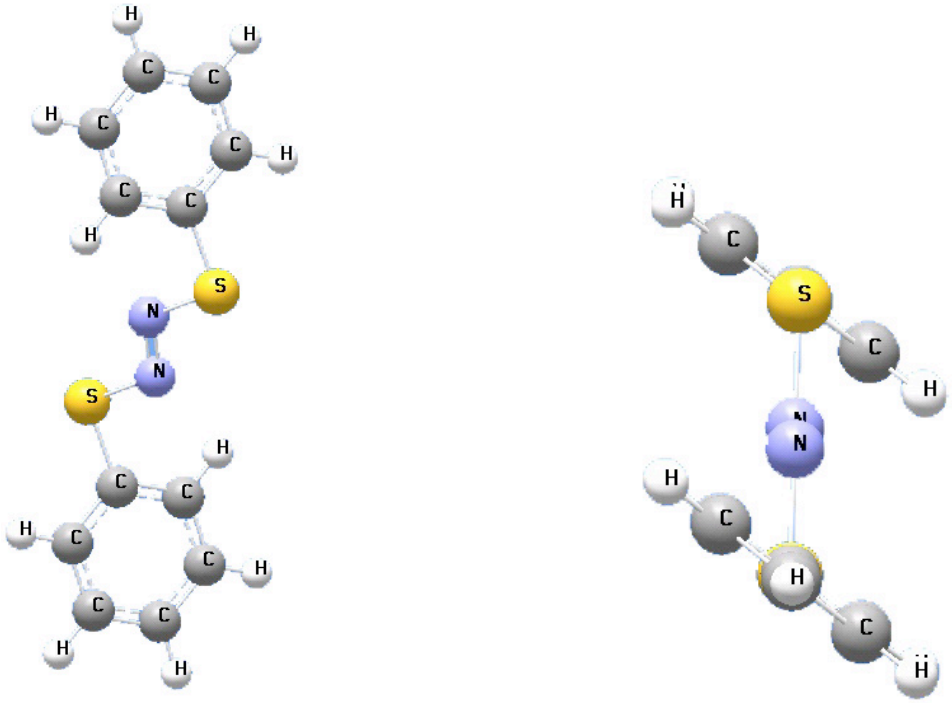

Figure 3.3. Final structural results for the geometry optimizations of **10**.

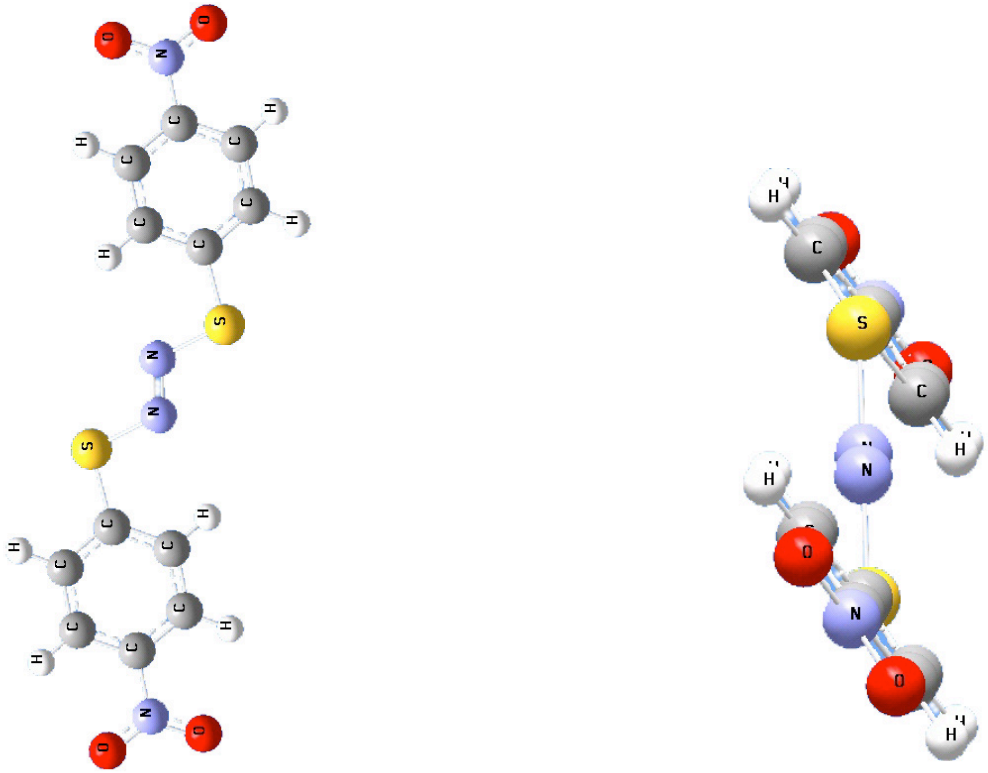

Figure 3.4. Final structural results for the geometry optimizations of **11**.

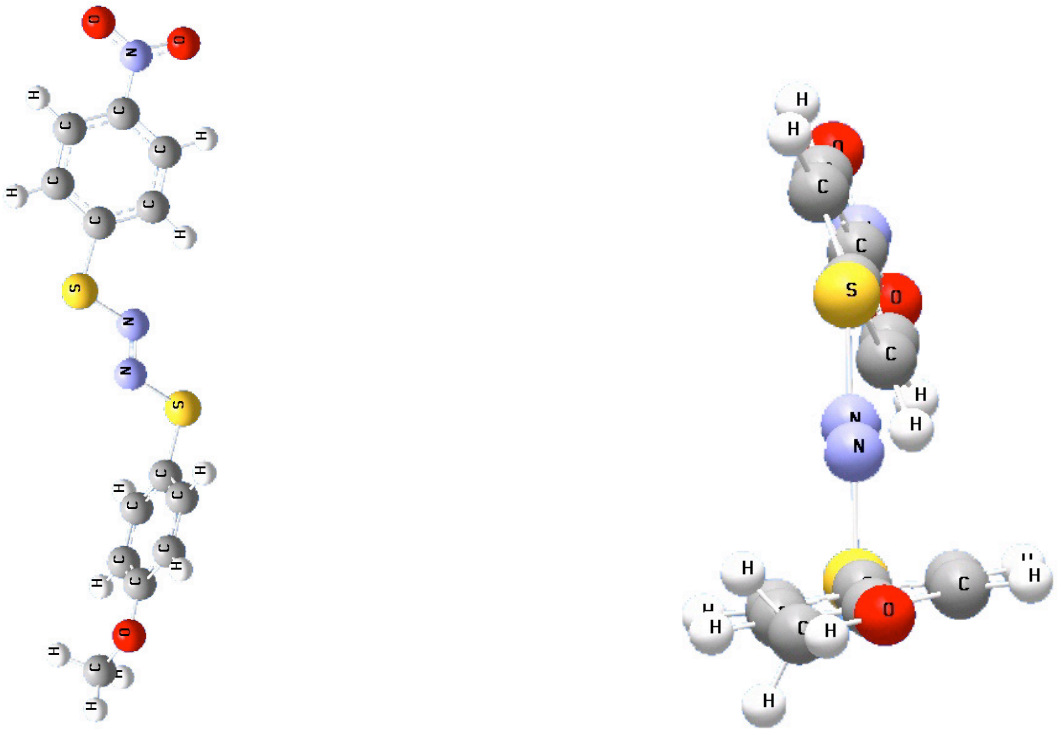

Figure 3.5. Final structural results for the geometry optimizations of **12**.

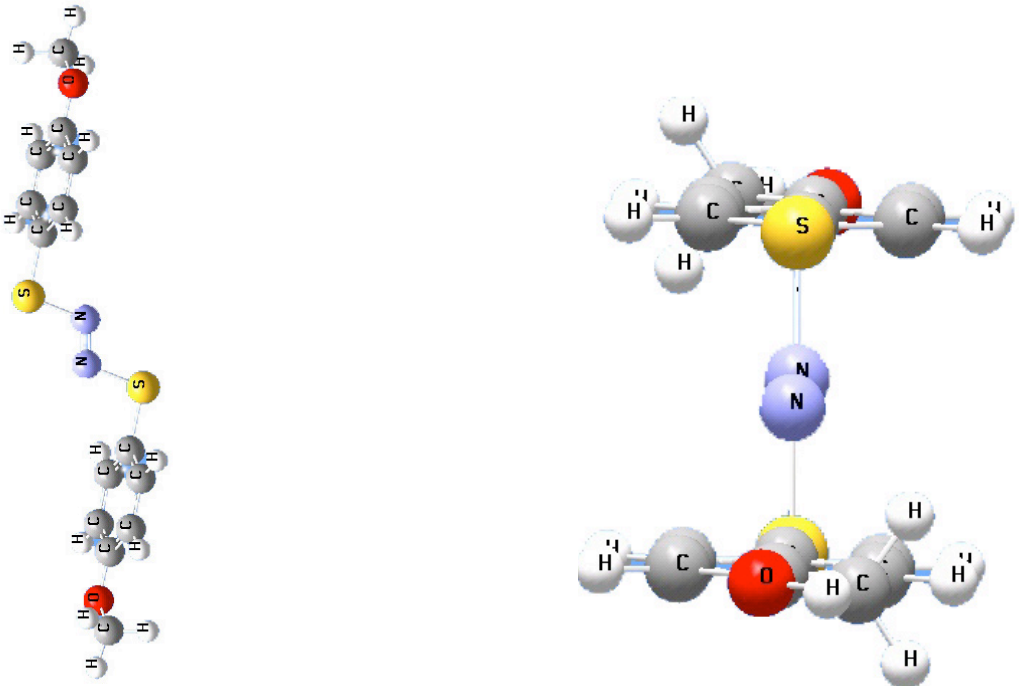

Figure 3.6. Final structural results for the geometry optimizations of **13**.

plane of the SNNS group, 35.1° and 20.8° respectively. As a matter of fact one of the dihedral angles of **12** (20.8°) is almost identical to the dihedral angle of **14** ($\phi C_{(18)}C_{(23)}N_{(2)}N_{(1)}$) (20.7°) which is a part of the conjugated system (Appendix 1).

The difference between the dihedral angles of structures **10** through **14** is seen in the degree of the conjugation of S-N=N-S with the aryl substituents. The Highest Occupied Molecular Orbitals (HOMO) of **10** - **14** serve as a good illustration of this process (Appendix 2, Figure A2.10 - A2.14). In the systems of **10** - **12,** we clearly see an interaction between one of the lone pairs of the sulfur atom with the aryl groups. However in **13** and in the methoxyphenyl part of **12** and **14,** there is no evidence of the contribution of the S lone pair (S LP(2)) to the system's conjugation.

3.5 COMPUTATIONAL EVALUATION OF STRUCTURES **1** - **9**

Computational evaluation of structures **1** - **8** required a different approach than the calculations of the previously discussed systems. The former systems do not have a chemical model with experimentally obtained structural data that would be electronically and/or chemically close to the discussed systems with at least one S-N=N bond. Therefore, we had to turn to the oxygen analog of the bis-thiodiazenes, *trans*-di-*tert*-butyl hyponitrite (**9**) that had previously been studied (11).

Computational results for the geometry optimization of **9** are reported in the Table 3.4.

Initial steps of the geometry optimization of **9** were identical to those of **14** (Section 3.3). In order to choose the best route for the LDBS step of the geometry optimization of **1**, **2**, **5**, **6**, **7** and **8,** we performed an experiment in which we varied the diffuse function distribution about **9** (Table 3.4). Column 1 includes results based on the calculations without diffuse functions. In column 2 – we placed two diffuse functions on each oxygen

atom and one diffuse function on each nitrogen atom. In column 3 – one diffuse function on atom oxygen atom. In column 4 – one diffuse function on each nitrogen atom. In column 5 – one diffuse function on each oxygen atom. In column 6 – one diffuse function on each nitrogen atom. Based on the obtained results we came to the conclusion that it is essential not to put any diffuse functions on oxygen and carbon atoms, but it is essential to assign one diffuse function to the nitrogen atoms.

Computational results for the geometry optimization of **1** - **8** are reported in Table 3.5.

Comparing structural differences of *Z*-HSN=NSH (**1**) and *E*-HSN=NSH (**2)** versus *cis*-HON=NOH (**3**) and *trans*-HON=NOH (**4**), we noticed that the structural differences between *Z* and *E* conformations of the former pair is greater than that between the *cis* and *trans* conformations of the latter pair. Such differences can be explained by long-range interactions between sulfur atoms of the *Z* conformation (84) (see Appendix 2).

Substitution of the fluorine atoms on **6** for hydrogen atoms on one of the sides of the molecule affected the S-N bonds due to push-pull effects, which will be discussed later in Chapter 4.

Table 3.6 summarizes delocalization of one of sulfur's lone pairs. It shows that the delocalization for the present structures is smaller than that for structures **10** through **14**. Also, we would like to point out that delocalization of one of oxygen's lone pairs in **9** is smaller in comparison than the delocalization of sulfur's lone pair in the analogous structures. This observation underlines the greater polarizability of sulfur's lone pairs.

3.6 CONCLUDING REMARKS

The most important observation that was made in the course of the computational evaluation of the above-mentioned systems was the importance of the proper utilization of the diffuse functions during the LDBS step in the calculations.

Structural studies have demonstrated that a substitution group on the sulfur atom plays a crucial role in determining the geometry of the system.

Table 3.1. Crystallographic results and B3LYP calculations of the structure of $NO_2PhN{=}NSPhOMe$ (**14**). Bond lengths are reported in Angstroms (Å) and molecular angles are reported in degrees (°).

	calculated results[a]						experimental results[b]	
	1	2	3	4	5	6	7	8
N-S	1.752	1.738	1.738	1.721	1.719	1.721	1.726(3)	1.729(6)
S-C	1.780	1.777	1.774	1.766	1.768	1.767	1.755(3)	1.762(6)
N-C	1.424	1.422	1.423	1.422	1.421	1.425	1.433(4)	1.440(6)
N=N	1.252	1.244	1.244	1.244	1.245	1.244	1.236(4)	1.245(6)
∠CSN	98.9	99.2	99.2	99.5	99.5	99.4	99.6	
∠SNN	112.1	112.9	112.9	113.5	113.4	113.5	110.3	
ϕ NSCC	98.5	85.6	85.8	85.5	86.5	79.2	69.0	

[a] Column 1: 6-311(d,p) basis set was assigned to all atoms of **14**.

Columns 2 – 6: for basis set descriptions, see Appendix 1, Figure A1.14.

[b] Column 7 is experimental X-ray data, Column 8 is experimental data corrected for thermal motion.

Table 3.2. B3LYP calculations on the structures of **10** - **13**. Bond lengths are reported in Angstroms (Å) and molecular angles are reported in degrees (°).

	10	**11**	**12**	**13**
	PhSNNSPh	$NO_2PhSNNSPhNO_2$	$NO_2PhSNNSPhOMe$[a]	MeOPhSNNSPhOMe
S-N	1.745	1.727	1.737	1.762
S-N			1.742	
N=N	1.232	1.237	1.234	1.228
S-C	1.772	1.771	1.763	1.766
S-C			1.742	
∠NNS	113.2	113.1	112.7	113.0
∠NNS			113.3	
∠NSC	98.5	99.1	99.7	98.9
∠NSC			99.1	
ϕNNSC	179.6	178.6	176.5	179.9
ϕNNSC			179.2	
ϕNSCC	55.6	35.1	20.8	88.9
ϕNSCC			82.6	

[a] For $NO_2PhSNNSPhOMe$, the first line is for the $NO_2C_6H_4S$ part of the molecule, the second line is for the SC_6H_4OMe part.

Table 3.3. NLMO analysis of the delocalization of one of the sulfur's lone pairs of RS-NN-SR′ and of NO_2PhNNSPhOMe.

	10	**11**	**12**	**13**	**14**
R/R′:	Ph/Ph	NO_2Ph/PhNO_2	NO_2Ph/PhOMe[a]	MeOPh/PhOMe	NO_2PhNNSPhOMe
Total electron density on S lone pair (%)	90.33	87.54	87.88 90.00	91.97	87.96
Electron density of S lone pair delocalized					
to: C (nearest) (%)	1.24	2.31	2.94 0.71	0.74	0.73
to: C & H (next to the nearest C) (%)	1.29	4.74	3.85	0.78	1.50
to: N (nearest) (%)	3.40	3.64	2.69 4.34	3.12	5.10
to: N (remote) (%)	3.28	3.48	2.55 3.83	3.02	3.95
to: other S (%)	0.17	0.16	0.49 0.08	0.16	n/a

[a] For NO_2PhSNNSPhOMe, the first line is for the $NO_2C_6H_4S$ part of the molecule, the second line is for the SC_6H_4OMe part.

Table 3.4. B3LYP calculations for the structure of *tert*-BuONNO*tert*-Bu (**9**).
Bond lengths are reported in Angstroms (Å) and molecular angles are reported in degrees (°).

	calculated results[a]						experimental results[b]
	1	2	3	4	5	6	7
N=N	1.228	1.252	1.226	1.264	1.263	1.263	1.252(6)
N-O	1.384	1.444	1.396	1.386	1.387	1.387	1.380(6)
O-C	1.464	1.475	1.477	1.467	1.464	1.464	1.471(7)
∠ONN	107.9	107.6	107.8	107.9	107.7	107.7	106.5(3)
∠NOC	111.0	110.5	111.1	110.6	110.7	110.7	109.3(3)

[a] Columns 1- 6: for basis set descriptions, see Appendix 1, Figure A1.9.

[b] Column 7 is experimental X-ray data (11)

Table 3.5. B3LYP calculations on the structures **1** - **8**. Bond lengths are reported in Angstroms (Å) and molecular angles are reported in degrees (°).

	1	**2**	**3**	**4**	**5**	**6**	**7**	**8**
R/R′	(Z)H/H	(*E*)H/H	*cis*HO/OH	*trans*HO/OH	CH_3/CH_3	CF_3/CH_3[a]	CF_3/CF_3	*t*-Bu/*t*-Bu
S-N						1.741		
S(O)-N	1.772	1.732	1.406	1.395	1.722	1.718	1.730	1.715
N=N	1.253	1.279	1.253	1.259	1.276	1.235	1.232	1.276
S(O)-C(H)	1.348	1.349	0.969	0.969	1.806	1.818	1.824	1.851
S-C						1.807		
∠NNS(O)	121.5	113.3	114.4	107.5	114.4	112.6	113.2	114.9
∠NNS						114.3		
∠NS(O)C(H)	91.5	92.2	101.0	101.2	96.6	94.9	94.7	98.4
∠NSC						97.2		
ϕNNS(O)C(H)	180.0	180.0	180.00		180.0	180.0	180.0	180.0
ϕNNSC						180.0		

[a] For $CF_3SNNSCH_3$, the first line is for the CF_3S part of the molecule, the second line is for the SCh_3 part.

Table 3.6. NLMO analysis of the delocalization of one of the sulfur's lone pairs.

	1	**5**	**6**	**7**	**8**	**9**
R/R′:	(Z)H/H	CH_3/CH_3	CF_3/CH_3[a]	CF_3/CF_3	*t*-Bu/*t*-Bu	*t*-BuONNO*t*-Bu
Total electron density on S lone pair (%)	92.63	90.54	91.22 89.80	90.43	90.07	92.65
Electron density of S lone pair delocalized to: C (nearest) (%)	n/a	0.54	0.49 2.46	2.18	0.58	0.54
to: C & H (next to the nearest) (%)	n/a	0.36	0.64		0.85	0.57
to: N (nearest) (%)	3.18	4.03	4.63 2.47	3.25	4.13	2.98
to: N(remote) (%)	3.13	3.90	4.34 2.45	3.13	4.01	2.98
to: S (%)	0.11	0.25	0.51 0.09	0.16	0.24	0.90

[a] For $CF_3SNNSCH_3$, the first value is for the CF_3S part of the molecule, the second value is for the SCH_3 part.

CHAPTER 4

HYBRID DENSITY FUNCTIONAL INVESTIGATION OF BOND DISSOCIATION ENERGIES OF THE S-N BOND OF R-S-N=N-S-R SYSTEMS

4.1 INTRODUCTION

The range of chemical compounds that have sulfur–nitrogen bonds vary from heterocyclic compounds to metal complexes with sulfur-nitrogen ligands. Although there have been numerous studies on sulfur-nitrogen chemistry, the nature of these S-N bonds still is not completely understood.

Understanding the sulfur-nitrogen bond is very important for a variety of compounds. Especially intriguing is the investigation of sulfur–nitrogen chemistry with regard to its potential application for nitrogen fixation. In this respect, the study of S-N interactions in diazene, one of the possible intermediates in nitrogen fixation, could be very beneficial. Therefore it is essential to study such models that will help us to understand the role of substituent effects on the energies of S-N bonds.

Bis-thiodiazene compounds are valuable models for the investigation of the energies of sulfur-nitrogen bonds. Potentially, they could be important sources of thiyl radicals as are their thiodiazene counterparts, R-N=N-S-R'. Also, they could be important as chemical initiators that are capable of producing thiyl radicals. The quality of the thiodiazenes is based on the weakness of the S-N bond which is susceptible to homolytic decomposition under thermal or photolytic conditions (1,6,7,85). A theoretical study of

the influence of the substituent effects on the sulfur-nitrogen bond dissociation energies of the R-S-N=N-S-R seemed of great interest.

4.2 THEORETICAL METHODOLOGY OF THE CALCULATIONS OF THE HOMOLYTIC BOND DISSOCIATION ENERGIES

In this work we will define the term *bond dissociation energy* (BDE) as the quantity of energy that is required to cleave a given chemical bond into two radicals (85-88). Homolytic BDE can be expressed as the overall energy change for the reaction:

$$\text{R-S-N=N-S-R} \rightarrow \text{R-S}\bullet + \bullet\text{N=N-S-R}$$

Therefore, the BDE is:

$$\text{BDE} = E(\text{R-S}\bullet) + E(\bullet\text{N=N-S-R}) - E(\text{R-S-N=N-S-R})$$

Table 4.1 gives the total electronic energies of the systems and their fragments with zero-point energy corrections. Also, in bold, we present the BDE of the S-N bonds of the systems under study are given.

4.3 COMPUTATIONAL METHODS

The calculations were performed using Gaussian 98 revision A.7 software suite (55). As was described in Section 3.2 of this work, we used Hybrid Density Functional Theory – B3LYP for the energy calculations. LDBS method was used as it is described in Section 3.3. DiLabio and coworkers (76-79) applied LDBS method for the computational determination of the bond dissociation enthalpies, substituent effects in para-substituted phenols, solvation energies, activation energies, and proton and electron affinities. In their calculations they divided a molecule into several regions according to their priorities. They then assigned larger basis sets to the regions with higher priority and, consequently, smaller basis sets to the regions with lower priority. The priorities were

determined based on the points of interest. The point of interest in bond dissociation energy calculations would include, for example, those two atoms whose chemical bond was broken. The largest basis sets of the calculations would be assigned to those two atoms, and smaller basis sets or series of basis sets to the rest of the system. The main motivation of DiLabio and coworkers to use LDBS method was an attempt to bring computational cost down. We followed this methodology (Appendix 1).

4.4 COMPUTATIONAL EVALUATION OF BDE OF THIOLS

There were three systems chosen for the computational calibration: hydrogen sulfide, methanethiol, and thiophenol (benzenethiol). The results were encouraging:

$H\text{-}SH \rightarrow H\bullet + \bullet SH$ BDE = +89.32 kcal/mol (exptl: 91.2 ± 0.7 kcal/mol (107))

$H\text{-}SCH_3 \rightarrow H\bullet + \bullet SCH_3$ BDE = +84.38 kcal/mol (exptl: 87.31 ± 0.6 kcal/mol (107))

$H\text{-}SPh \rightarrow H\bullet + \bullet SPh$ BDE = +78.17 kcal/mol (exptl: 83.29 ± 1.9 kcal/mol (108))

The geometry optimizations of the thiols also were performed as was described in Section 3.2. Some results are given here.

For hydrogen sulfide:

S-H bond length is 1.3492 Å (exptl 1.3356 Å),

HSH angle is 92.42º (exptl 92.12º).

For methanethiol:

S-H bond length is 1.35 Å (exptl 1.34 Å),

C-S bond length is 1.828 Å (exptl 1.819 Å), C-H bond length is 1.09Å (exptl 1.09 Å),

HSC angle is 97.3º (exptl 96.5º) (33,34).

For thiophenol:

S–H bond length is 1.3817 Å,

C-S bond length is 1.821 Å,

HSC angle is 96.77º (experimental structural data were not conclusive (91,92)).

As we can see, our results demonstrate excellent agreement with the experimental values, thus validating our computational methodology.

4.5 ENERGIES OF THE STUDIED SYSTEMS. RESULTS AND ANALYSIS

The total energies of the studied systems (E_t) were calculated based on their fully optimized structures. There were no restrictions imposed on the systems with the exception of the diazenyl radicals, R-S-N=N•: structural restrictions were imposed on the S-N bond of these diazenyl radicals because the S-N bond of the thiodiazenyl radical is not stable and it is prone to spontaneous homolytic cleavage. Such behavior was observed for hyponitrous acid and a possibility of a concerted O-N bond cleavage has been studied (54).

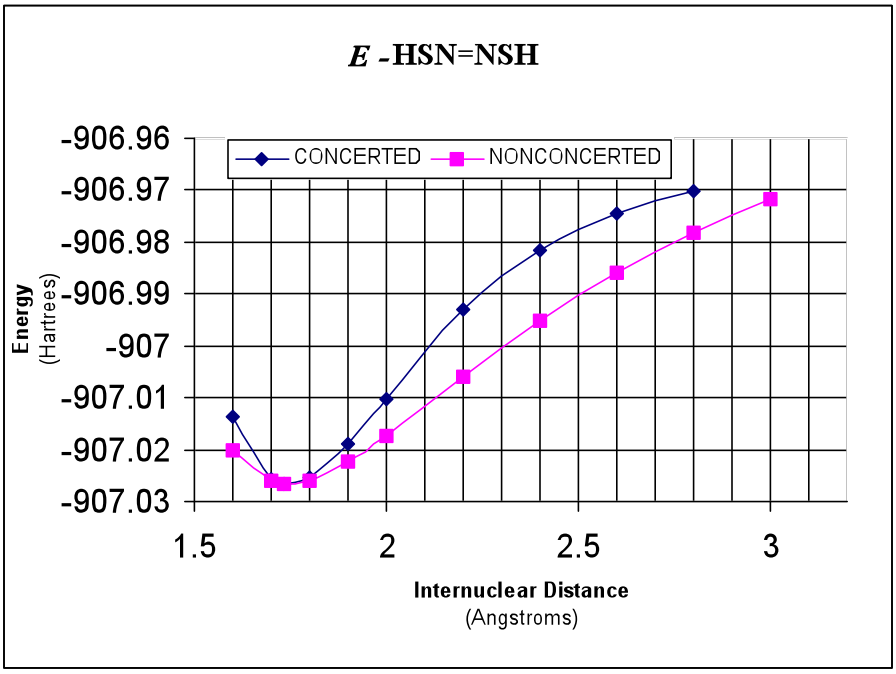

Figure 4.1. Comparison of the single (nonconcerted) and concerted S-N bond scissions, based on S-N internuclear distance.

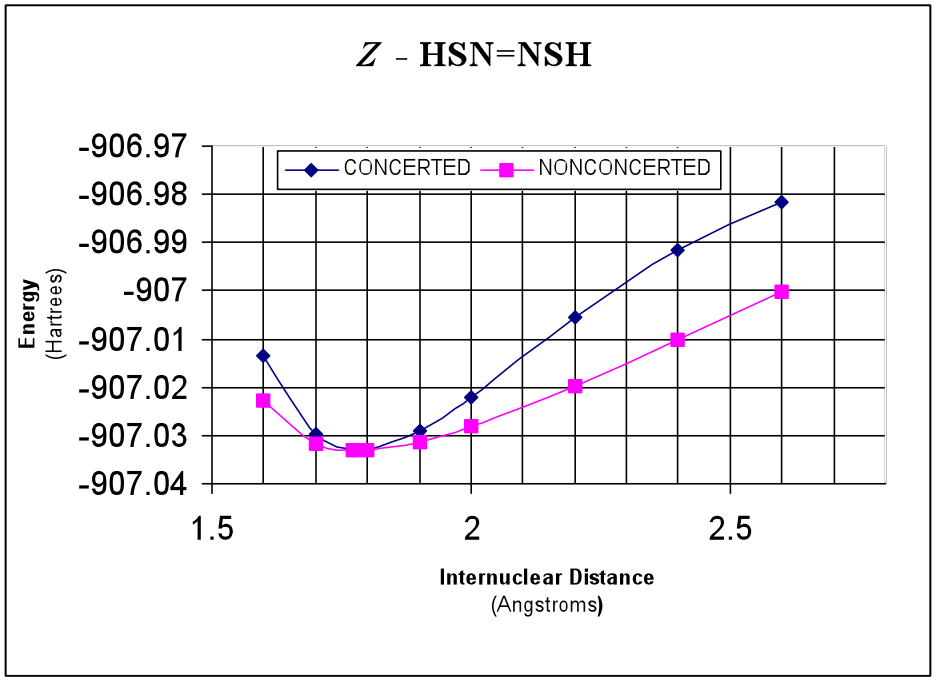

Figure 4.2. Comparison of the single (nonconcerted) and concerted S-N bond scissions, based on S-N internuclear distance.

Our calculations consisted of the study of *E* and *Z* conformations of HSNNSH. Calculations of each system consisted of two parts. The first part involved the study of the concerted decomposition of HSNNSH. For this first part, we elongated both S-N bonds stepwise, noting changes of the total energy of the systems. The second part involved elongation of only one of the S-N bonds. Changes in the total energies of the systems are reflected in the Figure 4.1 and Figure 4.2. Our results demonstrate that homolytic decomposition of both conformations of HSNNSH should follow a nonconcerted path.

The total energies of each system and their corresponding radicals, which include Zero Point Energy (ZPE) corrections, are presented in Table 4.1.

The results in Table 4.1 can be divided into three groups. The first group would include BDE's of the S-N bond of structures **1, 2, 5, 7** and **8**: their average BDE is ~ 29

kcal/mol. The second group consists of BDE's of **10** and **13** whose average value is ~ 16 kcal/mol. The last group would include **6**, **11**, **12**, and **14** whose BDE's significantly surpass that of the former two groups. To explain the differences between the BDE's of the above-mentioned groups we need to examine structural variations of the various compounds.

Let us begin our discussion with the first group of the molecules.

Molecules that belong to the first group are all symmetrical. Both of their sulfur atoms have identical substituents. It seems that electronegativities of the substituents do not play a significant role in strengthening the S-N bond. Indeed, the inductive effect that changes significantly among the compounds of this group is not crucial for the BDE of the S-N bond.

Results of the Natural Atomic Charges of the Natural Population Analysis (NBO 4.0 software suite) (82) are listed in the Table 4.3. These results show that the charge variance on the α-substituents of the sulfur atoms goes from +0.92009 of **7** (carbon of $CF_3SNNSCF_3$) to –0.82214 of **5** (carbon of $CH_3SNNSCH_3$). The charges are indicators of the influences of the inductive effects that are opposite in **7** and **5**. At the same time, electrical charges on the sulfur atoms remain at the same level, +0.44754 and +0.4304 respectively (Table 4.3). Furthermore, the BDE's of S-N of **7** and **5** are about the same, 28.37 kcal/mol and 28.04 kcal/mol (Table 4.1).

The inductive effect is graphically represented in Figure 4.3. In the structure on the left, both R and N have greater negative charge than S. In the structure on the right, R and S are more positively charged than the nitrogen atoms. Despite these two opposite types

of inductive effects, the systems' BDE does not differ to any significant degree (Table 4.1).

Figure 4.3. Directions for the inductive effect in the systems of study.

Therefore, we can see that the electron-withdrawing or electron-releasing inductive effect of the substituents does not affect the BDE of the S-N bond directly.

To understand the reason why all S-N BDE's are very close in value, we direct our attention to the charge distributions between S and N (Table 4.3). Natural Atomic Charge values of S and N do not vary greatly from system to system (with the exception of **1** for S). The average negative charge on N is - 0.36, and the average positive charge on S is + 0.44. The key point here lies in the difference between the charges of S and N. It was established that highly diffused sulfur lone pairs can considerably effect the resonance hybrid if S has a formal positive charge and if it is bonded to an electronegative group (94). In our case we have a range of charges going from + 0.44 on S to - 0.36 on N. This difference in charges is the result of the S-N bond's ~30% ionic character. One of the sulfur's lone pairs, which can be easily polarized, contributes to the electronic overlap between S and N (94).

The interaction between the sulfur's lone pair and the substituents R that results in the resonance structure **A** (Figure 4.4) diminishes repulsion between lone pairs of S and N. The resonance effect increases the positive charge on S which strengthens the S-N bond by partial 3*p*π-2*p*π interaction (94). The result of such interactions on the structures **1, 2, 5, 7, 8** and **9** could be expressed through resonance effect, as shown in Figure 4.4.

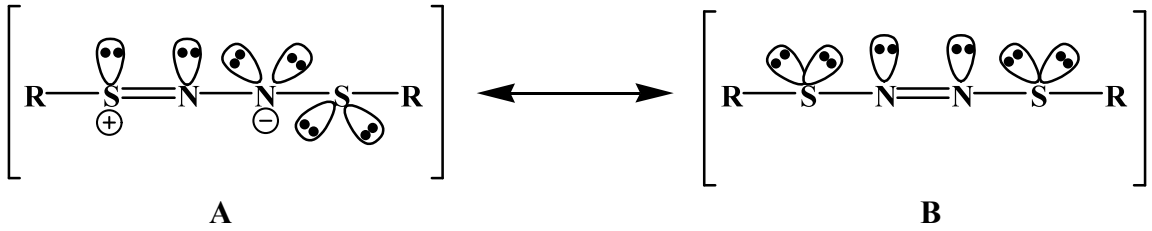

Figure 4.4. 3*p*π-2pπ interaction of the S-N bond could be expressed through resonance structure **A**. **B** is the main resonance contributor.

Our NBO NRT analysis demonstrated that such resonance hybrids have somewhere between 10% and 16% of the weight of the total structure (82).

The second group of the BDE's in Table 4.1 includes structures **10** and **13**. BDE's of this group are ~ 16 kcal/mol, only a fraction of the magnitude of the BDE's of the previous group. The reason again can be demonstrated by the resonance effect. Resonance contributions of the type that is depicted in Figure 4.4 have about 6% of the weight in structure **10,** and even less in structure **13** (the exact number could not be determined). Also, for this group there is a possibility for another resonance contributor incorporating the aromatic ring such as shown in Figure 4.5.

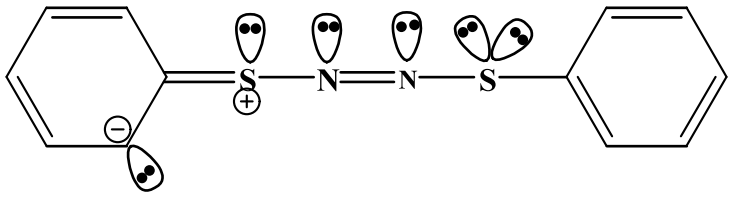

Figure 4.5. S-N bond as a part of the aryl ring conjugation.

Figure 4.5 is a demonstration of the interaction of one of the sulfur's lone pairs with π orbitals on the aryl ring. It was established that S can have a large neighboring effect on the β-carbons (94). In our case, S interacts not only with the β-carbons, but also with the

π orbitals on the aryl ring, thus establishing conjugation with it (Appendix 2, Figures A2.13.a – A2.13.d, Figures A2.14.a – A2.14.c). Also, it is important to note that sulfur lone pair (LP) delocalization in **13** occurs through the remote N to the remote aryl ring. An interaction of S's LP with the vicinal aryl group is of *gerade* character, which explains **13**'s perpendicularity of the aryl ring to the S-N=N-S plane (Appendix 2, Figures A2.13.a – A2.13.d).

The aryl substituents of **10** and **13** are mild electron-releasing groups. The combination of electron-donating inductive effect and sulfur's neighboring group effect diminishes the magnitude of the S-N π-bonding, reinforcing S-C π-bonding instead.

The third group of molecules includes one symmetrical system (**11**) and three asymmetrical ones (**6**, **12**, and **14**). Compound **11** stands out in this group because of its symmetry. It could be compared to **7** because the substituents on the sulfur atoms of both **7** and **11** are electron-withdrawing groups. The BDE of **11** however, is much higher than that in **7** (170.07 kcal/mol versus 28.04 kcal/mol). The source of this difference lies in the fact that the nitro group is an electron-withdrawing group that has the ability to increase its positive charge on sulfur (+ 0.52) promoting in that way resonance hybridization and establishing a π-bond with N atom. This gives an enhanced stability of the S-N bond of **11,** as compared with compounds of the first group, making the S-N bond part of the aryl ring conjugation, as shown in Figure 4.6.

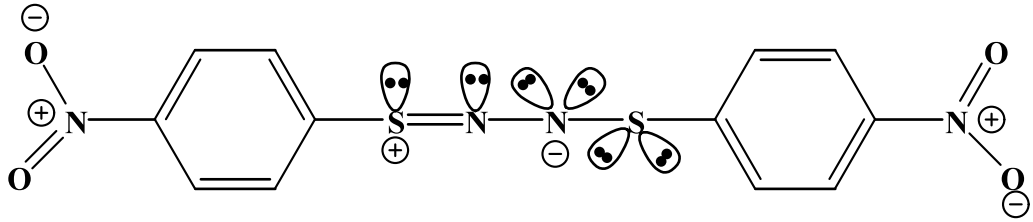

Figure 4.6. S-N bond as a part of the aryl ring conjugation.

The remaining systems of this group, **6**, **12**, and **14** are asymmetrical, with one part having an electron-releasing substituent on one sulfur atom and the other having an electron-withdrawing substituent on the other S.

An inspection of the HOMO (Appendix 2, Figure A2.6.a) of system **6** demonstrates that there is a strengthening of the S-N bond on the CF_3 side of the molecule, but this is absent in S-N bonds of **7**. According to Table 4.1 the BDE's of **6** are 64.42 kcal/mol and 31.46 kcal/mol as compared to the BDE of **7**, which is 28.04 kcal/mol.

A combination of the two inductive effects in **6**, the electron- releasing one and the electron-withdrawing one, has created a push-pull effect (also known as a captodative effect) (95-97) that increased the BDE's of both the S-N bonds of the molecule. A positive charge on one of the sulfur atoms and a negative charge on the adjacent nitrogen atom were increased, thus increasing delocalization of the S's LP and, therefore, reinforcing the S-N bond by creating additional resonance contributors with $3p\pi$-$2p\pi$ interactions. The magnitude of the other S-N bond remained at the same approximate level as in **7** because of the comparable difference of charges between the adjacent S and N.

Values for the BDE's of **12** and **14** are much larger than those of **6**. The magnitude of the values of the BDE's is a result of several things. One of them is the push-pull effect that, in combination with the structural specifics of **12** and **14,** increases the resonance effect that extends the conjugation of the S-N bonds with the aryl rings through the S 3d orbitals.

The qualitative and quantitative degree of S LP delocalization is demonstrated by the data on the Bond Dipole Moment analysis (Table 4.2), the Natural Localized Molecular Orbital analysis (Table 4.4), the Natural Bond Order Analysis (Table 4.5) (82), and the visualization of the MO (Appendix 2).

An analysis of the numerical data of the dipole moments, the distribution of charges, and the electron densities and energies of the various bonds of the systems, demonstrated that the only significant difference between all the systems of interest is the difference in the electron density and electron delocalization of one of the sulfur's lone pairs (S LP (2)) (see Tables 4.2 –4.5). The only visible correlation between systems **11**, **12**, and **14** with the highest values of BDE of the S-N bonds is the electron density on S LP 2, which is below 90% as opposed to the rest of the systems where this value is above 90%. The direction of the delocalization, and the hybrid character of the lone pair of systems **11**, **12**, and **14**, does not differ to any significant extent from those of **1**-**10** and **13**, with the exception of the delocalization to its vicinal carbon of the vicinal aryl group.

The figures in Appendix 2 depict MOs of our models. There is one visible qualitative difference between them. The MOs of the systems **10** through **14** (Appendix 2) show that there is conjugation between some carbons of the aryl groups and the S-N=N-S chain. Systems **1** through **9** lack this feature. We believe that a contribution from the electron delocalization of the S LP(2) to the global conjugation of the systems plays a crucial role in the increase or the decrease of the BDE's.

Also, we should point out that the discussed conjugation is of *ungerade*, π character. The fact that one lone pair of the sulfur atom is delocalized to a greater extent than the

other explains the asymmetrical "twist" of systems **10-12**, and **14** (Figures 3.3 – 3.6): the S LP(2) is delocalized to the opposite side of the vicinal aryl ring (Appendix 2).

All four systems display cross conjugation when the aryl carbons (primarily ipso and ortho) are not conjugated with the nitrogen atoms, but each of them are conjugated with the sulfur atom (98ϭ99). Here the electron-withdrawing effect of the *p*-nitro group in **11** induces conjugation and a push-pull effect (95-97) of the *p*-nitro group. The *p*-methoxy group of **12** and **14** create the most favorable electronic environment for the conjugation.

We have evidence that our models have hyperconjugation in its classical meaning. This involves σ, no-bond resonance structures. NBO resonance structure analysis (NRT) demonstrated that there is a significant contribution of hyperconjugation to the overall structure. On average we have 4% per system of the total weight of all resonance structures, as depicted in Figure 4.7.

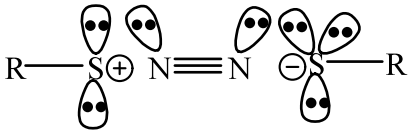

Figure 4.7. Hyperconjugation of the systems of study.

Another example of hyperconjugation (reverse hyperconjugation) of system **6** and **7** that contributes about 2% of the resonance weight per resonance structure is shown in Figure 4.8.

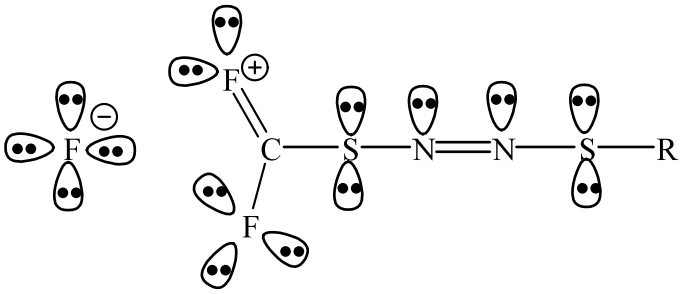

Figure 4.8. Reverse conjugation of **6** and **7**.

4.6 FURTHER VERIFICATION

As a final step we decided to further verify our BDE calculations. For this purpose we designed the following set of reactions.

pNO_2 ArS–NNSAr *p*NO_2 → *p*NO_2 ArS• + •NNSAr *p*NO_2 BDE = +170.07 kcal/mol

pNO_2 ArS• + •NNSAr *p*OMe → *p*NO_2 ArS–NNSAr *p*OMe -BDE = -237.33 kcal/mol

*p*MeOArS• + •NNSAr *p*NO_2 → *p*MeOArS–NNSAr *p*NO_2 -BDE = -230.73 kcal/mol

*p*MeOArS–NNSAr *p*OMe → *p*MeOArS• + •NNSAr *p*OMe BDE = +14.22 kcal/mol

The total of the BDEs of the reactions above are -283.77 kcal/mol. This value is based on the separate calculations of the total electronic energies of the whole systems and their corresponding free radicals. The following manipulation is based only on the total electronic energies of the whole systems. These two sets of reactions should have the same value, if there is no significant energy underestimation of the whole systems and no significant spin contamination in the free radicals.

The control set of the following reactions must match the above value:

pNO_2 ArS–NNSAr *p*NO_2 + *p*MeOArS–NNSAr *p*OMe → 2 *p*MeOArS–NNSAr *p*NO_2

BDE = E_t (2× -1688.00371H of *p*MeOArS–NNSAr *p*NO_2) – E_t (-1778.003235 H of *p*NO_2 ArS–NNSAr *p*NO_2 + -1597.551959H of *p*MeOArS–NNSAr *p*OMe) =

-0.452226H

Then, -0.452226H × 627.5095 kcal/H = -283.776 kcal/mol

This excellent agreement between the two reactions described above demonstrates that there was very little spin contamination during the calculations and there was negligible amount of underestimation of the calculations of the total energies. This gives validation of our results.

Table 4.1. Total Energies, Fragment Energies, and Bond Dissociation Energies (BDE) of the S-N bonds of RS-NN-SR′ systems[a].

	1	**2**	**5**	**6**	**7**	**8**	**9**	**10**	**11**	**12**	**13**	**14**
R/R′:	(*Z*)H/H	(*E*)H/H	CH_3/CH_3	CF_3/CH_3	CF_3/CF_3	CMe_3/CMe_3	other[b]	Ar/Ar	$NO_2Ph/PhNO_2$	$NO_2Ph/PhOMe$	MeOPh/PhOMe	other[c]
RSNNSR	-907.027	-907.033	-985.593	-1283.505	-1581.355	-1221.282	-575.254	-1369.005	-1778.003	-1688.004	-1597.552	-1289.598
RSNN·	-508.220	-508.222	-547.502	-845.409	-845.409	-665.346	-342.324	-739.237	-943.609	-943.609	-853.513	-545.320
RSNN·				-547.502						-853.513		
RS·	-398.765	-398.765	-438.046	-735.901	-735.901	-555.888	-232.881	-629.739	-834.123	-834.123	-744.016	-744.016
RS·				-438.046						-744.016		
RS-NNSR	**26.38**	**28.78**	**28.37**	**31.46**	**28.04**	**29.65**	**30.93**	**17.90**	**170.07**	**237.33**	**14.22**	**164.54**
				64.42[d]						**230.73**[e]		

[a] Total system energies (electronic energies plus ZPE) are reported in Hartrees. BDE are shown in bold and are reported in kcal/mol.

[b] *t*-BuONNO*t*-Bu; [c] $NO_2ArNNSArOMe$; [d] BDE of CF_3S-$NNSCH_3$, [e] BDE of MeOArS-$NNSArNO_2$

Table 4.2. Bond Dipole Moments of the RSNNSR systems.

Compound	S-N		S-C		N=N		N=N		N-C	
	NLMO	***NBO***	***NLMO***	***NBO***	***NLMO***	***NBO***	***NLMO***	***NBO***	***NLMO***	***NBO***
HSNNSH, **1**	1.61	1.36	1.97	1.99						
MeSNNSMe, **5**	1.68	1.45	0.27	0.23	0	0	0	0		
$CF_3SNNSMe$[a], **6**	1.40/1.16	1.72/1.41	0.46/0.38	0.28/0.21	0.02	0.02	1.4	1.2		
$CF_3SNNSCF_3$, **7**	1.53	1.26	0.42	0.34	0	0	0	0		
t-BuSNNStBu, **8**	1.56	1.36	0.28	0.16	0	0	0	0		
t-BuONNOtBu, **9**	0.54	0.67	1.7	1.73						
PhSNNSPh, **10**	1.57	1.28	0.38	0.27						
$NO_2ArSNNSArNO_2$, **11**	1.53	1.29	0.47	0.35	0	0	0	0		
$NO_2ArSNNSArMeO$[a], **12**	1.65/1.47	1.37/1.21	0.35/0.25	0.50/0.39	0.45/0.45	0.54/0.51				
MeOArSNNSArMeO, **13**	1.61	1.29	0.39	0.30	0	0	0	0		
$MeOArSNNArNO_2$, **14**	1.32	1.31	0.37	0.27	0.16	0.09	0.58	0.1	0.84	0.69

[a] In the asymmetrical systems, the first value is for the left side of the molecular formula as written.

Table 4.4. NLMO analysis of the S LP (2) of RSNNSR′.

	1	**5**	**6**[c]	**7**	**8**	**9**	**10**	**11**	**12**[c]	**13**	**14**[c]
R/R′:	(*Z*)H/H	CH_3/CH_3	CF_3/CH_3	CF_3/CF_3	*t*Bu/*t*Bu	other[a]	Ph/Ph	NO_2/NO_2	NO_2/OMe	MeO/MeO	other[b]
Total electron density on S lone pair (%)	92.63	90.54	91.22 89.80	90.43	90.07	92.65	90.33	87.54	87.88 90.00	91.97	87.96
Electron Density of S lone pair delocalized											
to: N(nearest) (%)	3.18	4.03	4.63	3.25	4.13	2.98	3.40	3.64	2.69	3.12	5.10
hybrid character (%)	p100	p100	2.47 p98 d2	p98 d2	p98 d2	p100	p98 d2	p98 d2	4.34 p100/p98 d2	p98 d2	p98 d2
to: N(remote) (%)	3.13	3.90	4.34	3.13	4.01	2.98	3.28	3.48	2.55	3.02	3.95
hybrid character (%)	p100	p100	2.45 p99 d1	p99 d1	p99 d1	p100	p99 d1	p99 d1	3.83 p98;d2/ p99;d1	p99 d1	p99 d1
to: other S(O) (%)	0.11	0.25	0.51	0.16	0.24	0.90	0.17	0.16	0.49	0.16	n/a
hybrid character (%)	p100	p66;d33 f1	0.09 p91;d9 p12d87 f1	p100	p73;d27	p92;d8	p69;d31	p64;d36	0.08 p92;d8 p18d81 f1	p64;d36	
to: C(nearest) (%)	n/a	0.54	0.49	2.18	0.58	0.54	1.24	2.31	2.94	0.74	0.73
hybrid character (%)		p90d10	2.46 p88d12 p96d4	p96d4	p95d5	p98d8	p97 d3	p99d1	0.71 p100 p96d4	p96d4	p96d4
C(other) (%) hybrid character (%)	n/a	H:0.35772 s100	H:0.64 s100		0.85 s40p59d1	2C:2x0.286 s38 p60d2	1.287 s28/ 44p55/ 100d0/3	4.74 s5/7 p92/100 d0/2	2.91/0.941 s3p97/ s62p37d1	0.391/0.390 s66 p34	1.5 s60 p40

[a] *t*-BuONNO*t*-Bu; [b] NO_2ArNNSArOMe; [c] In the asymmetrical systems, the first value is for the left side of the molecular formula as written.

Table 4.5. Natural Bond Orbital Analysis.

Compound	S-N		S-C(H)		N-N		N-N		S LP (1)		S LP (2)		N LP (1)	
	Occup.	*Energy*	*Occup.*	*Energy*	*Occup.*	*Energy*	*Occup.*	*Energy*	*Occup.*	*Energy*	*Occup.*	*Energy*	*Occup.*	*Energy*
(*Z*)HSNNSH, **1**	1.96632	-0.6748	1.98874	-0.57428	1.99474	-1.03522	1.98874	-0.41216	1.99907	-0.67698	1.85255	-0.2794	1.97751	-0.49990
$CH_3SNNSCH_3$, **5**	1.96485	-0.6575	1.98912	-0.60125	1.99290	-1.01257	1.98874	-0.39247	1.99501	-0.64566	1.81354	-0.2484	1.97291	-0.47842
$CF_3SNNSCH_3$, **6**	1.95622	-0.6612	1.98901	-0.61999	1.99555	-1.07636	1.99164	-0.66116	1.98890	-0.70762	1.82631	-0.2837	1.96779	-0.52575
$CH_3SNNSCF_3$, **6**	1.95606	-0.6798	1.97562	-0.66045	1.99555	-1.07636	1.99164	-0.66115	1.99347	-0.66995	1.80522	-0.2689	1.96801	-0.51639
$CF_3SNNSCF_3$, **7**	1.95379	-0.6909	1.97484	-0.67167	1.99516	-1.10221	1.99155	-0.45673	1.98931	-0.72470	1.81034	-0.29960	1.96647	-0.54363
t-BuSNNS*t*-Bu, **8**	1.96454	-0.6525	1.96328	-0.56711	1.99442	-0.98219	1.99168	-0.38438	1.99042	-0.64442	1.80477	0.23829	1.96824	-0.47752
t-BuONNO*t*-Bu, **9**	1.97788	-0.8182	1.98383	-0.79471	1.99577	-0.38732	1.98852	-0.99267	1.98202	-0.63206	1.85492	-0.3117	1.97797	-0.47461
PhSNNSPh, **10**	1.94817	-0.6310	1.97851	-0.63833	1.99506	-1.05105	1.99185	-0.40801	1.98527	0.65231	1.80909	-0.2504	1.96747	-0.49746
$NO_2PhSNNSPhNO_2$, **11**	1.95601	-0.68894	1.97755	-0.68646	1.99470	-1.08586	1.98815	-0.44718	1.98796	-0.68678	1.75425	-0.28786	1.96764	-0.53368
NO_2 PhSNNSPhOMe, **12**	1.94735	-0.64647	1.97823	-0.65197	1.99506	-1.06025	1.98925	-0.42937	1.98453	-0.66323	1.80930	-0.2599	1.96811	-0.50815
$MeOPhSNNSPhNO_2$, **12**	1.95520	-0.66000	1.97950	-0.67136	1.99506	-1.06025	1.98925	-0.42937	1.98602	-0.67307	1.75890	-0.2714	1.96594	-0.51591
MeOPhSNNSPhOMe, **13**	1.94260	-0.6038	1.97832	-0.63032	1.99520	-1.04386	1.99298	-0.39626	1.98408	-0.64252	1.84130	-0.2377	1.96875	-0.48873
NO_2 PhNNSPhOMe, **14**	1.96844	-0.6638	1.97880	-0.64962	1.99258	-1.02677	1.94626	-0.40533	1.98413	-0.65847	1.76605	-0.2583	1.97326	-0.50457

Table 4.3. Natural Atomic Charge (Summary of Natural Population Analysis).

Compound	S(O)	S(O)	N	N	C(H)	C(H)
HSNNSH, **1**	0.20617	0.20617	-0.34617	-0.34617	0.14000	0.14000
MeSNNSMe, **5**	0.43040	0.43040	-0.36582	-0.36583	-0.82214	-0.82214
$CF_3SNNSMe$, **6**	0.46738	0.41863	-0.35597	-0.33268	0.91719	-0.83834
$CF_3SNNSCF_3$, **7**	0.44754	0.44754	-0.32393	-0.32393	0.92009	0.92009
t-BuSNNStBu, **8**	0.44676	0.44676	-0.39127	-0.39127	-0.17485	-0.17485
t-BuONNOtBu, **9**	-0.40139	-0.40139	0.03831	0.03831	0.27345	0.27345
PhSNNSPh, **10**	0.46443	0.46443	-0.33875	-0.33875	-0.24887	-0.24887
NO2ArSNNSArNO2, **11**	0.52280	0.52280	-0.34857	-0.34857	-0.19027	-0.19027
NO2ArSNNSArMeO, **12**	0.47066	0.51759	-0.31186	-0.36855	-0.29337	-0.21934
MeOArSNNSArMeO, **13**	0.43042	0.43042	-0.33269	-0.33269	-0.29131	-0.29131
$MeOArSNNArNO_2$, **14**	0.50817	n/a	-0.32287	-0.23411	-0.29535	-0.11210

CHAPTER 5

SUMMARY AND CONCLUSIONS

The primary objective of this research was to study the effect of substituents, R, on the structure and the stabilities of RSNNSR systems. There were ten systems studied, using various combinations of R = H, CH_3, CF_3, *tert*-Butyl, C_6H_6, *p*-$NO_2C_6H_6$, *p*-$CH_3OC_6H_6$.

The calculations were performed using Gaussian 98 revision A.7 software suite.

For the calculations, we employed Hybrid Density Functional Theory (HDFT) -- B3LYP method with Becke's three-parameter non-local exchange and Lee-Yang-Parr's non-local correlation functionals.

Computational methodology was based on the locally dense basis set approach (LDBS) that assigns various levels of the basis sets according to the previously calibrated results that could be correlated to experimental data.

For the initial step we used only STO-3G basis set, with three primitive Gaussians. Subsequent steps involved Pople-type basis sets: split valence shell double-zeta plus polarization 3-21G* basis set, split valence shell double-zeta plus double polarization 6-31G(*, *) basis set, and split valence shell triple-zeta plus double polarization 6-311G(*, *) basis set. Polarization and diffusion functions of 6-31G and 6-311G basis sets have been adjusted according to the computational needs. The search for the global minima of the potentials was verified by screening the frequency calculations of the systems for imaginary frequencies.

The most significant differences that could be found among molecules **1-8** and **10-13** reside in their S-N bonds and, for **10-13**, in their NSCC dihedral angles. The most noticeable difference in dihedral angles is between structures **13** (φNSCC = 88.9°) and **12** (φNSCC = 20.8°).

A Natural Localized Molecular Orbital (NLMO) analysis, which is part of the NBO 4.0 software package, helped us to understand the structural variations of **10-13**. The NLMO analysis shows that the principal difference among systems **10** through **13** is in the degree of delocalization of one of the lone pairs of the sulfur atoms.

The lone pair delocalization has π-bonding character that is a result of the interaction of sulfur's 3p orbital with 2p orbitals of the neighboring atoms and/or with π-orbitals of the aryl ring. This delocalization accounts for 10% - 12% of the electronic density of sulfur's lone pair to the neighboring atoms. The most crucial direction of the electron delocalization that influences the dihedral angle ϕNSCC is a donation of the electron density to the aryl group. Dihedral angles of **11** and **12** are closest to the plane of the SNNS group, 35.1° and 20.8° respectively.

The study of the stabilities of the RSNNSR systems concentrated on the investigation of the homolytic Bond Dissociation Energy (BDE) of the S-N bonds.

The total energies of the RSNNSR systems and the total energies of the RS• and •NNSR radicals were calculated. The difference of the sum of the total energies of both radicals and the total energy of the whole system yielded the BDE of the S-N bond.

The BDE's of the S-N bonds range from 14.22 kcal/mol for **13** to 237.33 kcal/mol for **12**.

All molecules were divided into three groups according to the magnitude of the BDE of S-N bond.

The first group includes BDE's of the S-N bond of structures **1, 2, 5, 7** and **8**: their average BDE is ~ 29 kcal/mol. The second group consists of BDE's of **10** and **13** whose average value is ~ 16 kcal/mol. The last group would include **6**, **11**, **12**, and **14** whose BDE's significantly surpass that of the former two groups. To explain the differences between the BDE's of the above-mentioned groups we need to examine structural variations of the various compounds.

Molecules that belong to the first group are all symmetrical. Both of their sulfur atoms have identical substituents. It seems that electronegativities of the substituents do not play a significant role in strengthening the S-N bond. Indeed, the inductive effect that changes significantly among the compounds of this group is not crucial for the BDE of the S-N bond.

The charge distributions between S and N play the important role in the stability of the S-N bond. Natural Atomic Charge values of S and N do not vary greatly from system to system (with the exception of **1** for S). The average negative charge on N is - 0.36, and the average positive charge on S is + 0.44. The key point here lies in the difference between the charges of S and N. It was established that highly diffused sulfur lone pairs can considerably effect the resonance hybrid if S has a formal positive charge and if it is bonded to an electronegative group. In our case we have a range of charges going from + 0.44 on S to - 0.36 on N. This difference in charges is the result of the S-N bond's ~30% ionic character. One of the sulfur's lone pairs, which can be easily polarized, contributes to the electronic overlap between S and N.

The second group of the BDE's in Table 4.1 includes structures **10** and **13**. BDE's of this group are ~ 16 kcal/mol. The reason for the lower BDE of this group lies in the fact that the aryl substituents of **10** and **13** are mild electron-releasing groups. The combination of electron-donating inductive effect and sulfur's neighboring group effect diminishes the magnitude of the S-N π-bonding, reinforcing S-C π-bonding instead.

The third group of molecules includes one symmetrical system (**11**, BDE = 170.07 kcal/mol) and three asymmetrical ones (**6**, BDE = 31.46 kcal/mol and 64.42 kcal/mol; **12**, BDE = 237.33 kcal/mol and 230.73 kcal/mol; **14**, BDE = 164.54 kcal/mol). The BDE's of this group range from 31.46 kcal/mol (**6**) to 237.33 kcal/mol (**12**). There are several explanations for this.

The source of the high BDE of **11** (170.07 kcal/mol) could be explained by the fact that the nitro group is an electron-withdrawing group that has the ability to increase its positive charge on sulfur (+ 0.52), thus promoting resonance hybridization and establishing a π-bond between S and N. In addition, an interaction of one of the sulfur's lone pairs with the π system of the aryl ring gives an enhanced stability of the S-N bond of **11**, making the S-N bond part of the aryl ring conjugation.

The remaining systems of this group, **6**, **12**, and **14** are asymmetrical, with one part having an electron-releasing substituent on one sulfur atom and the other having an electron-withdrawing substituent on the other S. The resultant push-pull effect (captodative effect) increased the BDE's of both the S-N bonds of the molecules. A positive charge on one of the sulfur atoms and a negative charge on the adjacent nitrogen atom were increased, thus increasing delocalization of the S's LP and, therefore,

reinforcing the S-N bond by creating additional resonance contributors with 3*p*π-2*p*π interactions.

Therefore, we can conclude that in order to better stabilize the S-N bond in a RSNNSR system it is important:

-to have the charge difference between the substituents and S atom,

-to have substituents that would make the β-effect possible, and,

-to have the push-pull effect.

Reference List

1. Zollinger, H. *Diazo Chemistry I. Aromatic and Heteroaromatic Compounds.* VCH: Weinheim, 1994; Vol. 1.

2. Reiding, J.; de Kok, A. J.; de Graaff, R. A. G.; Romers, C. *Acta Cryst. B* **1976**, *32* 2643.

3. Zollinger, H. *Diazo Chemistry II. Aliphatic, Inorganic and Organometallic Compounds.* VCH: Weinheim, 1995; Vol. 2.

4. van Zwet, H.; Kooyman, E. C. *Recl. Trav. Chim. Pays-Bas.* **1967**, *86,* 993.

5. van Beek, L. K. H.; van Beek, J. R. G. C. M.; Boven, J.; Schoot, C. J. *J. Org. Chem.* **1971**, *36*, 2194.

6. Haub, E. K.; Lizano, A. C.; Noble, M. E. *J. Am. Chem. Soc.* **1992**, *114,* 2218.

7. Brokken-Zijp, J.; Bogaert, H. V. D. *Tetrahedron* **1973**, *29,* 4169.

8. Haub, E. K.; Richardson, J. F.; Noble, M. E. *Inorg. Chem.* **2002**, *31,* 4926.

9. Regitz, M.; Maas, G. *Diazo Compounds. Properties and Synthesis.* Academic.: Orlando, 1986.

10. Greene, R. L.; Grant, P. M.; Street, G. B. *Phys. Rev. Lett.* **1975**, *31,* 89.

11. Ogle, C. A.; van der Kooi, K. A.; Mendenhall, G. D.; Lorprayooth, V.; Cornilsen, B. C. *J. Am. Chem. Soc.* **1982**, *104,* 5114.

12. Kurmaev, E. Z.; Poteryaev, A. I.; Anisimov, V. I.; Karla, I.; Moewes, A.; Schneider, B.; Neumann, M.; Ederer, D. L.; Lyubovskaya, R. N. *Physica C.* **1999**, *321,* 191.

13. *Transition Metal Sulfur Chemistry. Biological and Industrial Significance.*, Stiefel, E. I.; Matsumoto, K., Eds.; American Chemical Society: Washington, DC, 1996.

14. Sanchez-Delgado, R. A. *Organometallic Modeling of the Hydrodesulfurization and Hydrodenitrogenation Reactions.* Kluwer Academic: Dordrecht, 2002.

15. Rakowski DuBois, M.; Jagirdar, B.; Noll, B.; Dietz, S. *Transition Metal Sulfur Chemistry. Biological and Industrial Significance.*, Stiefel, E. I.; Matsumoto, K., Eds; American Chemical Society: Washington, DC, 1996; p. 269.

16. Eagle, A. A.; Thomas, S.; Young, C. G. *Transition Metal Sulfur Chemistry. Biological and Industrial Significance.*, Stiefel, E. I.; Matsumoto, K., Eds.; American Chemical Society: Washington, DC, 1996; p. 324.

17. Tatsumi, K.; Kawaguchi, H. *Transition Metal Sulfur Chemistry. Biological and Industrial Significance.*, Stiefel, E. I.; Matsumoto, K., Eds.; American Chemical Society : Washington, DC, 2002; p. 336.

18. Stiefel, E.I. *Transition Metal Sulfur Chemistry. Biological and Industrial Significance.*, Stiefel, E. I.; Matsumoto, K., Eds.; American Chemical Society : Washington, DC, 2002; p. 2.

19. Sakane, G.; Shibahara, T. *Transition Metal Sulfur Chemistry. Biological and Industrial Significance.*, Stiefel, E. I.; Matsumoto, K., Eds.; American Chemical Society : Washington, DC, 2002; pp. 336.

20. Coucouvanis, D.; Han, J.; Moon, N. *J. Am. Chem. Soc.* **2002**, *124*, 216.

21. Burgess, B. K.; Lowe, D. J. *Chem. Rev.* **1996**, *96,* 2983.

22. Einsle, O.; Tezcan, F. A.; Andrade, S. L. A.; Schmid, B.; Yoshida, M.; Howard, J. B.; Rees, D. C. *Science.* **2002**, *297,* 1696.

23. Sellmann, D.; Sutter, J. *Transition Metal Sulfur Chemistry. Biological and Industrial Significance.* Stiefel, E. I.; Matsumoto, K., Eds.; American Chemical Society : Washington DC, 1996; p. 101.

24. Atkins, P. W.; Friedman, R. S. *Molecular Quantum Mechanics.;* 3d ed.; Oxford University Press.: Oxford, 1997.

25. Szabo, A.; Ostlund, N. S. *Modern Quantum Chemistry. Introduction to Advanced Electronic Structure Theory.;* Dover Publications: Mineola, 1989.

26. Atkins, P. W. *Physical Chemistry;* 6th ed.; H.Freeman and Sumanas: Oxford, 1998.

27. Koch, W.; Holthausen, M. C. *A Chemist's Guide to Density Functional Theory.* 2nd ed.; Wiley-VCH: New York, 2001.

28. Frisch, Æ.; Frisch, M. J. *Gaussian 98 User's Reference;* Gaussian: Pittsburgh, 1999.

29. Seminario, J. M.; Politzer, P. *Modern Density Functional Theory. A tool for Chemistry.;* Elsevier: Amsterdam, 1995.

30. Jensen, F. *Introduction to Computational Chemistry.* John Wiley & Sons: Chichester, 1999.

31. Sadlej, J. *Semi-Empirical Methods of Quantum Chemistry.* Ellis Horwood: Chichester, 1985.

32. Eckart, C. E. *Phys. Rev.* **1939**, *36*, 878.

33. Dirac, P. A. M. *The Principles of Quantum Mechanics.;* 4th ed.; Oxford University: London, 1958.

34. Hohenberg, P.; Kohn, W. *Phys. Rev.* **1964**, *136,* B864.

35. Kohn, W.; Sham, L. J. *Phys. Rev.* **1965**, *140,* A1133.

36. Becke, A. D. *J. Chem. Phys.* **1988**, *88,* 1053.

37. Burke, K.; Perdew, J. P.; Wang, Y. *Electronic Density Functional Theory: Recent Progress and New Directions.* Dobson, J. F.; Vignale, G.; Das, M. P., Eds; Plenum: 1998; Chapter 7, p. 81.

38. Perdew, J. P. *Electronic Structure of Solids.* Ziesche, P.; Eschrig, H., Eds; Akademie Verlag.: Berlin, 1991; Chapter 1, p. 11.

39. Perdew, J. P.; Chevary, J. A.; Vosko, S. H.; Jackson, K. A.; Pederson, M. R.; Singh, D. J.; Fiolhais, C. *Phys. Rev. B.* **1992**, *46,* 6671.

40. Perdew, J. P.; Chevary, J. A.; Vosko, S. H.; Jackson, K. A.; Pederson, M. R.; Singh, D. J.; Fiolhais, C. *Phys. Rev. B.* **1993**, *48,* 4978.

41. Lee, C.; Yang, W.; Parr, R. G. *Phys. Rev. B.* **1988**, *37,* 785.

42. Miehlich, B.; Savin, A.; Stoll, H.; Preuss, H. *Chem. Phys. Lett.* **1989**, *157,* 200.

43. Becke, A. D. *J. Chem. Phys.* **1993**, *98,* 5648.

44. Boys, S. F. *Proc. R. Soc. (London)* **1950**, *542,* A200.

45. Binkley, J. S.; Pople, J. A.; Hehre, W. J. *J. Am. Chem. Soc.* **1980**, *102,* 939.

46. Gordon, M. S.; Binkley, J. S.; Pople, J. A.; Pietro, W. J.; Hehre, W. J. *J. Am. Chem. Soc.* **1982**, *104,* 2797.

47. Hehre, W. J.; Radom, L.; Schleyer, P. v. R.; Pople, J. A. *Ab Initio Molecular Orbital Theory;* Wiley: New York, 1986.

48. Pietro, W. J.; Francl, M. M.; Hehre, W. J.; Defrees, D. J.; Pople, J. A.; Binkley, J. S. *J. Amer. Chem. Soc.* **1982**, *104,* 5039.

49. Dobbs, K. D.; Hehre, W. J. *J. Comp. Chem.* **1986**, *7,* 359.

50. Dobbs, K. D.; Hehre, W. J. *J. Comp. Chem.* **1987**, *8,* 861.

51. Dobbs, K. D.; Hehre, W. J. *J. Comp. Chem.* **1987**, *8,* 880.

52. Almog, J.; Barton, D. H. R.; Magnus, P. D.; Norris, R. K. *J. Chem. Soc., Perkin Trans.* **1974**, *1*, 853.

53. Barton, D. H. R.; Blair, I. A.; Magnus, P. D.; Norris, R. K. *J. Chem. Soc., Perkin Trans.* **1973**, *1*, 1031.

54. Brown, R. E.; Mendenhall, G. D. *Int. J. Quantum Chem. Quantum Chem. Symposium.* **1987**, *21,* 603.

55. Frisch, M. J.; Trucks, G. W.; Schlegel, H. B.; Scuseria, G. E.; Robb, M. A.; Cheeseman, J. R.; Zakrzewski, V. G.; Montgomery, Jr. J. A.; Stratmann, R. E.; Burant, J. C.; Dapprich, S.; Millam, J. M.; Daniels, A. D.; Kudin, K. N.; Strain, M. C.; Farkas, O.; Tomasi, J.; Barone, V.; Cossi, M.; Cammi, R.; Mennucci, B.; Adamo, C.; Clifford, S.; Ochterski, J.; Petersson, G. A.; Ayala, P. Y.; Cui, Q.; Morokuma, K.; Malick, D. K.; Rabuck, A. D.; Raghavachari, K.; Foresman, J. B.; Cioslowski, J.; Ortiz, J. V.; Baboul, A. G.; Stefanov, B. B.; Liu, G.; Liashenko, A.; Piskorz, P.; Komaromi, I.; Gomperts, R.; Martin, R. L.; Fox, D. J.; Keith, T.; Al-Laham, M. A.; Peng, C. Y.; Nanayakkara, A.; Gonzalez, C.; Challacombe, M.; Gill, P. M. W.; Johnson, B. G.; Chen, W.; Wong, M. W.; Andres, J. L.; Head-Gordon, M.; Replogle, E. S.; Pople, J. A. *Gaussian 98 (Revision A.7)* [Computer Program]. Gaussian: Pittsburgh, 1998

56. Vosko, S. H.; Wilk, L.; Nusair, M. *Can. J. Phys.* **1980**, *58,* 1200.

57. Hertwig, R. H.; Koch, W. *Chem. Phys. Lett.* **1997**, *268,* 345.

58. Collins, J. B.; Schleyer, P. v. R.; Binkley, J. S.; Pople, J. A. *J. Chem. Phys.* **1976**, *64,* 5142.

59. Hehre, W. J.; Stewart, R. F.; Pople, J. A. *J. Chem. Phys.* **2002**, *51,* 2657.

60. Foresman, J. B.; Frisch, AE. *Exploring Chemistry with Electronic Structure Methods.;* Gaussian: Pittsburgh, 1996.

61. Pulay, P. *J. Comp. Chem.* **2002**, *3,* 556.

62. Hehre, W. J.; Stewart, R. F.; Pople, J. A. *J. Chem. Phys.* **1969**, *51,* 2657.

63. Binkley, J. S.; Pople, J. A.; Hehre, W. J. *J. Am. Chem. Soc.* **1980**, *102,* 939.

64. Binning, Jr. R. C.; Curtiss, L. A. *J. Comput. Chem.* **1990**, *11*, 1206.

65. Ditchfield, R.; Hehre, W. J.; Pople, J. A. *J. Chem. Phys.* **1971**, *54,* 724.

66. Gordon, M. S. *Chem. Phys. Lett.* **1980**, *76,* 163.

67. Hariharan, P. C.; Pople, J. A. *Theor. Chim. Acta.* **1973**, *28,* 213.

68. Hariharan, P. C.; Pople, J. A. *Mol. Phys.* **1974**, *27,* 209.

69. Hehre, W. J.; Ditchfield, R.; Pople, J. A. *J. Chem. Phys.* **1972**, *56,* 2257.

70. Curtis, L. A.; McGrath, M. P.; Blaudeau, J.-P.; Davis, N. E.; Binning, Jr. R. C.; Radon, L. *J. Chem. Phys.* **1995**, *103,* 6104.

71. Krishnan, R.; Binkley, J. S.; Pople, J. A. *J. Chem. Phys.* **1980**, *72,* 650.

72. Krishnan, R.; Binkley, J. S.; Seegar, R.; Pople, J. A. *J. Chem. Phys.* **1980**, *72,* 650.

73. McGrath, M. P.; Radon, L. *J. Chem. Phys.* **1991**, *94,* 511.

74. Wachters, A. J. H. *J. Chem. Phys.* **1970**, *52,* 1033.

75. Jensen, J. H.; Gordon, M. S. *J. Comput. Chem.* **1991**, *12*, 421.

76. DiLabio, G. A.; Pratt, D. A.; LoFaro, A. D.; Wright, J. S. *J. Phys. Chem. A* **1999**, *103,* 1653.

77. DiLabio, G. A. *J. Phys. Chem.* **1999**, *A103,* 11414.

78. DiLabio, G. A.; Pratt, D. A. *J. Phys. Chem.* **2000**, *A 104,* 1938.

79. DiLabio, G. A.; Wright, J. S. *Chem. Phys. Lett.* **1998**, *297,* 181.

80. Huber, H.; Diel, P. *Mol. Phys.* **1985**, *54,* 725.

81. Chesnut, D. B.; Moore, J. *J. Comput. Chem.* **1989**, *10,* 648.

82. Glendening, E. D.; Badenhoop, J. K.; Reed, A. E.; Carpenter, J. E.; Bohmann, J. A.; Morales, C. M.; Weinhold, F. *NBO 5.0.* [Computer Program]. Theoretical Chemistry Institute, University of Wisconsin: Madison, 2001

83. Oae, S. *Theochem.* **1988**, *186* 321.

84. Bondi, A. *J. Phys. Chem.* **1964**, *68,* 441.

85. McMillen, D. F.; Golden, D. M. *Annu. Rev. Phys. Chem.* **1982**, *33,* 493.

86. March, J. *Advanced Organic Chemistry. Reactions, Mechanisms, and Structure.* 4th ed.; John Wiley & Sons: New York, 1992.

87. Klotz, I. M.; Rosenberg, R. M. *Chemical Thermodynamics. Basic Theory and Methods.* 4th ed.; Krieger Publishing Company: Malabar, Florida, 1991.

88. Kellogg, R. M. *Methods In Free-Radical Chemistry.* Huyser, E. S., Ed.; Marcel Dekker: New York, 2002; Vol. 2, p. 2.

89. Nicovich, J. M.; Wang, S.; Kreutter, K. D.; van Dijk, C. A.; Wine, P. H. *J. Phys. Chem.* **1992**, *96,* 2518.

90. McMillen, D. F.; Golden, D. M. *Annu. Rev. Phys. Chem.* **1982**, *33,* 493.

91. BelBruno, J. J. *J. Mol. Struct. (Theochem).* **1995**, *358,* 125.

92. Tsuda, K.; Yamazaki, A.; Kanno, M.; Onda, M. *The 17th International Conference on High Resolution Molecular Spectroscopy.* Prague, 2002; Chapter H65.

93. Bartlett, R. J. *Int. J. Quantum Chem. Quantum Chem. Symposium.* **1987**, *21,* 603.

94. Oae, S. *Organic Sulfur Chemistry: Structure and Mechanism.;* CRC : Boca, 1991; Vol. 1.

95. Manatt, S. L.; Roberts, J. D. *J. Org. Chem.* **2002**, *24,* 1336.

96. Breslow, R.; Kivelevich, D.; Mitchell, M. J.; Fabian, W.; Wendel, K. *J. Am. Chem. Soc.* **1965**, *87,* 5132.

97. Hess, B. A.; Schaad, L. J. *J. Org. Chem.* **1976**, *41,* 3058.

98. Phelan, N. F.; Orchin, M. *J. Chem. Educ.* **1968**, *45,* 633.

99. Hopf, H. *Angew. Chem.* **1984**, *96,* 947.

APPENDICES

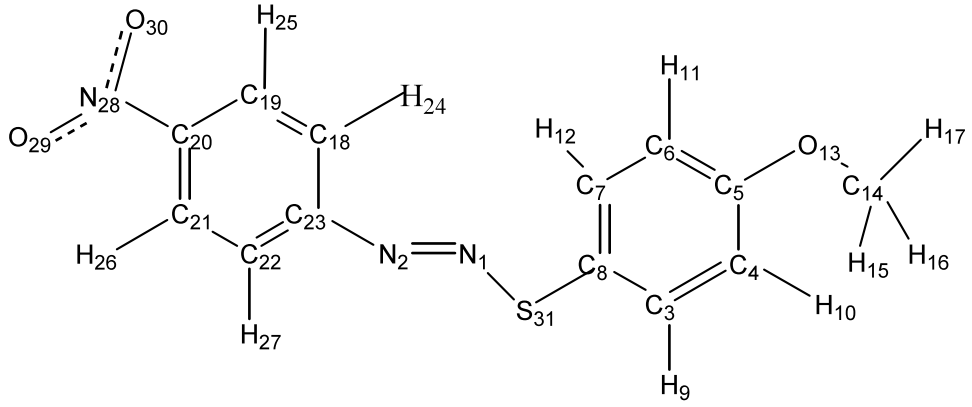

Figure 14.1.

Compare to the Figure 14.

See Table 3.1. Basis set assignments to the atoms of 14. Numbers correspond to the atomic centers of 14 as it appears in the Gaussian input files.

For 2*:

H 0
6-31d
****
C N O S 0
6-311+(2d,p)
****

For 3*:

H 0
3-21g*
****
O 0
6-31++(2d,2p)
****
N S 0
6-311++(2d,2p)
****

C 0
6-31++(2d,2p)
****

For 4*:

9 10 11 12 15 16 17 24 25 26 27 0
3-21g*
****
13 28 29 30 0
6-31++(d,p)
****
1 2 0
6-311+(2df,2pd)
****
31 0
6-311++(3df,3pd)
****
3 4 5 6 7 8 14 18 19 20 21 22 23 0
6-31(d,p)
****

For 5*:

9 10 11 12 15 16 17 24 25 26 27 0
3-21g*
****
13 28 29 30 0
6-31+(d,p)
****
1 2 31 0
6-311++(3df,3pd)
****
3 4 5 6 7 8 14 18 19 20 21 22 23 0
6-31+(d,p)
****

For 6*:

9 10 11 12 15 16 17 0
3-21g*
****
24 25 26 27 0
6-31+(d)

****
13 28 29 30 0
6-31++(d,p)
****
1 2 0
6-311+(2df,2pd)
****
31 0
6-311++(3df,2pd)
****
3 4 5 6 7 14 18 19 20 21 22 0
6-31(d,p)
****
8 0
6-31+(2d,2p)
****
23 0
3-21g*
****

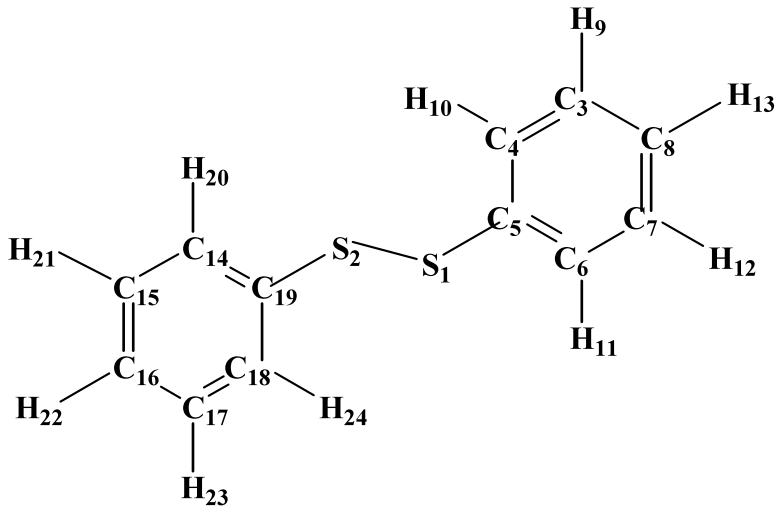

Figure 10.1.

Compare to Figure 10.

Basis set assignments to the atoms of 10. Numbers correspond to the atomic centers of 10 as it appears in the Gaussian input files.

```
1 0
6-311++(3df,2pd)
++++
3 4 5 6 7 0
6-31(d,p)
****
2 0
6-31+(2d,2p)
****
8 9 10 11 12 0
3-21g*
****
```

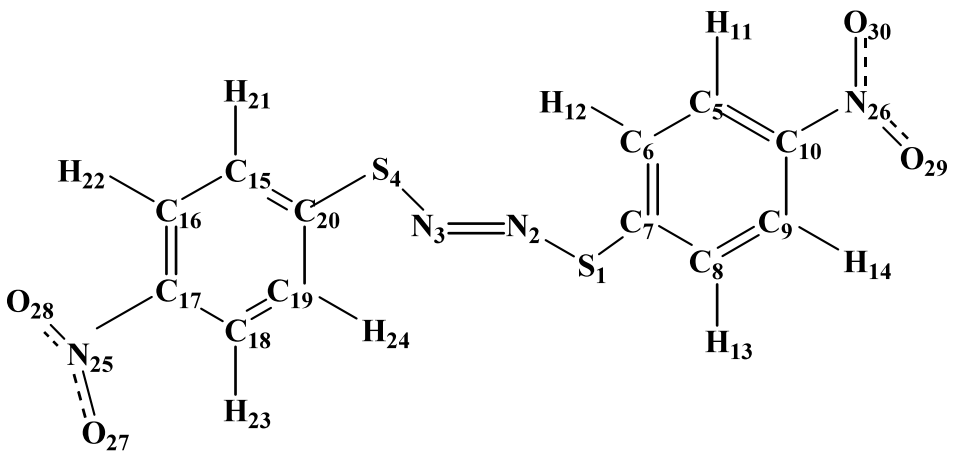

Figure 11.1.

Compare to Figure 11.

Basis set assignments to the atoms of 11. Numbers correspond to the atomic centers of 11 as it appears in the Gaussian input files.

```
11 12 13 14 21 22 23 24 0
3-21g*
****
5 6 8 9 10 15 16 17 18 19 0
6-31(d,p)
****
7 20 0
6-31g+(2d,2p)
****
25 26 27 28 29 30 0
6-31+(d,p)
****
1 4 0
6-311++(3df,2pd)
****
2 3 0
6-311+(2df,2pd)
****
```

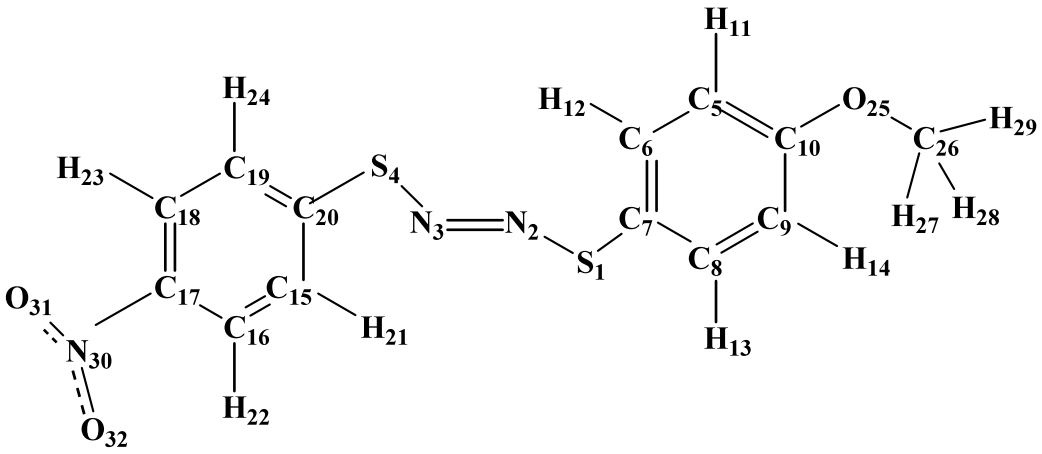

Figure 12.1.

Compare to Figure 12.

Basis set assignments to the atoms of 12. Numbers correspond to the atomic centers of 12 as it appears in the Gaussian input files.

```
11 12 13 14 27 28 29 0
3-21g*
****
21 22 23 24 0
3-21g*
****
5 6 8 9 10 15 16 17 18 19 26 0
6-31(d,p)
****
7 20 0
6-31+(2d,2p)
****
25 30 31 32 0
6-31+(d,p)
****
1 4 0
6-311++(3df,2pd)
****
2 3 0
6-311+(2df,2pd)
****
```

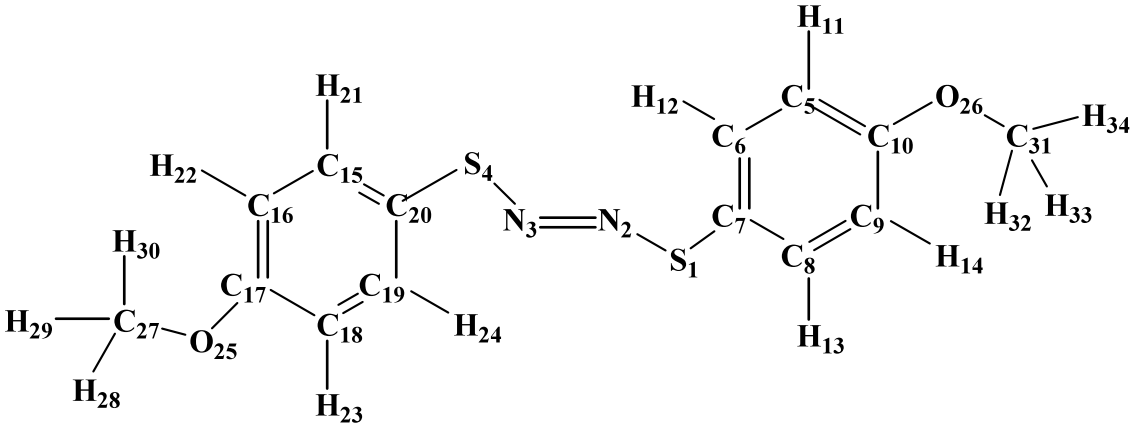

Figure 13.1.

Compare to Figure 13.

Basis set assignments to the atoms of 13. Numbers correspond to the atomic centers of 13 as it appears in the Gaussian input files.

```
1 4 0
6-311++(3df,2pd)
****
2 3 0
6-311+(2df,2pd)
****
5 6 8 9 10 15 16 17 18 19 0
6-31(d,p)
****
7 20 0
6-31+(2d,2p)
****
25 26 0
6-31(d,p)
****
11 12 13 14 21 22 23 24 28 29 30 32 33 34 0
3-21g*
****
27 31 0
3-21g*
****
```

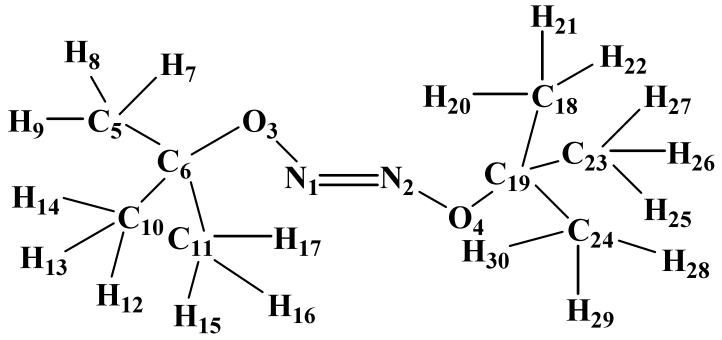

Figure 9.1.

Compare to the Figure 9.

Basis set assignments to the atoms of 9. Numbers correspond to the atomic centers of 9 as it appears in the Gaussian input files.

For 1*:

```
7 8 9 12 13 14 15 16 17 20 21 22 25 26 27 28 29 30 0
3-21g*
****
1 2 0
6-311g(2df,2pd)
****
3 4 0
6-311g(2df,2pd)
****
6 19 0
6-31g(2d,2p)
****
5 10 11 18 23 24 0
6-31g(2d,2p)
****
```

For 2*:

```
7 8 9 12 13 14 15 16 17 20 21 22 25 26 27 28 29 30 0
3-21g*
****
1 2 0
6-311g+(2df,2pd)
****
3 4 0
```

```
6-311g++(2df,2pd)
****
6 19 0
6-31g(2d,2p)
****
5 10 11 18 23 24 0
6-31g(2d,2p)
****
```

For 3*:

```
7 8 9 12 13 14 15 16 17 20 21 22 25 26 27 28 29 30 0
3-21g*
****
1 2 0
6-311g(2df,2pd)
****
3 4 0
6-311g+(2df,2pd)
****
6 19 0
6-31g(2d,2p)
****
5 10 11 18 23 24 0
6-31g(2d,2p)
****
```

For 4*:

```
7 8 9 12 13 14 15 16 17 20 21 22 25 26 27 28 29 30 0
3-21g*
****
1 2 0
6-311g+(2df,2pd)
****
3 4 0
6-311g(2df,2pd)
****
6 19 0
6-31g(2d,2p)
****
5 10 11 18 23 24 0
6-31g(2d,2p)
****
```

For 5*:

```
7 8 9 12 13 14 15 16 17 20 21 22 25 26 27 28 29 30 0
3-21g*
****
1 2 0
6-311g(3df,2pd)
****
3 4 0
6-311g+(3df,2pd)
```

```
****
6 19 0
6-31g(2d,2p)
****
5 10 11 18 23 24 0
6-31g(2d,2p)
****
```

For 6*:

```
7 8 9 12 13 14 15 16 17 20 21 22 25 26 27 28 29 30 0
3-21g*
****
1 2 0
6-311g+(2df,2pd)
****
3 4 0
6-311g(3df,2pd)
****
6 19 0
6-31g(2d,2p)
****
5 10 11 18 23 24 0
6-31g(2d,2p)
****
```

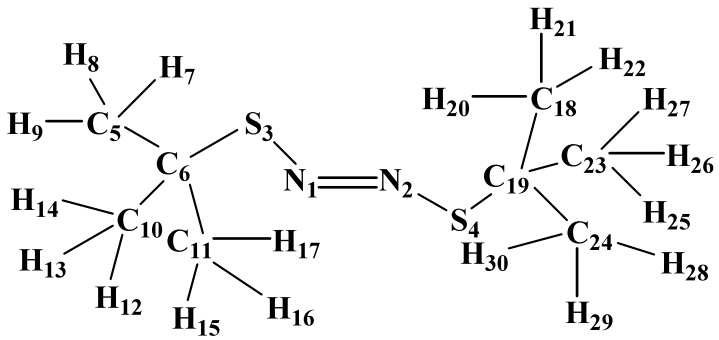

Figure 8.1.

Compare to the Figure 8.

Basis set assignments to the atoms of 9. Numbers correspond to the atomic centers of 9 as it appears in the Gaussian input files.

```
3 4 0
6-311(3df,2pd)
****
1 2 0
6-311+(2df,2pd)
****
5 10 11 18 23 24 0
6-31(d,p)
****
6 19 0
6-31(2d,2p)
****
7 8 9 12 13 14 15 16 17 20 21 22 25 26 27 28 29 30 0
3-21g*
****
```

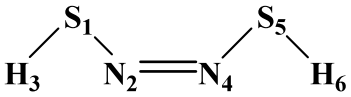

Figure 1.1.

Compare to the Figure 1.

Basis set assignments to the atoms of 1. Numbers correspond to the atomic centers of 1 as it appears in the Gaussian input files.

```
1 5 0
6-311g(3df,2pd)
****
2 4 0
6-311g+(2df,2pd)
****
3 6 0
3-21g*
****
```

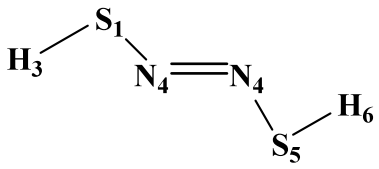

Figure 2.1.

Compare to the Figure 2.

Basis set assignments to the atoms of 2. Numbers correspond to the atomic centers of 2 as it appears in the Gaussian input files.

```
1 5 0
6-311g(3df,2pd)
****
2 4 0
6-311g+(2df,2pd)
****
3 6 0
3-21g*
****
```

Figure 3.1.

Compare to the Figure 3.

Basis set assignments to the atoms of 3.

```
N 0
6-311g+(2df,2pd)
****
O 0
6-311g(3df,2pd)
****
H 0
3-21g*
****
```

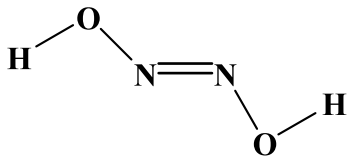

Figure 4.1.

Compare to the Figure 4.

Basis set assignments to the atoms of 4.

```
N 0
6-311g+(2df,2pd)
****
O 0
6-311g(3df,2pd)
****
H 0
3-21g*
****
```

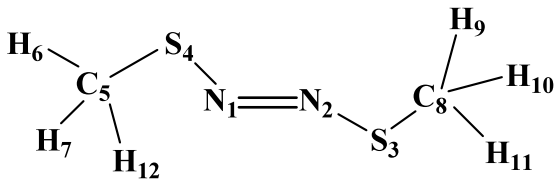

Figure 5.1.

Compare to the Figure 5.

Basis set assignments to the atoms of 5. Numbers correspond to the atomic centers of 5 as it appears in the Gaussian input files.

```
1 2 0
6-311g+(2df,2pd)
****
3 4 0
6-311g(3df,2pd)
****
5 9 0
6-31g(2d,2p)
****
6 7 8 10 11 12 0
3-21g*
****
```

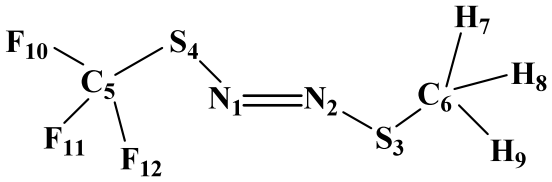

Figure 6.1.

Compare to the Figure 6.

Basis set assignments to the atoms of 6. Numbers correspond to the atomic centers of 6 as it appears in the Gaussian input files.

```
4 3 0
6-311++(3df,2dp)
****
1 2 0
6-311+(2df,2pd)
****
5 6 0
6-31+(2d,2p)
****
7 8 9 0
3-21g*
****
10 11 12 0
6-311++(2d,2p)
****
```

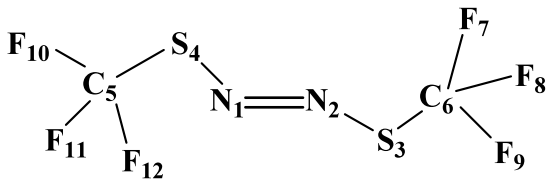

Figure 7.1.

Compare to the Figure 7.

Basis set assignments to the atoms of 7. Numbers correspond to the atomic centers of 7 as it appears in the Gaussian input files.

```
4 3 0
6-311++(3df,2dp)
****
1 2 0
6-311+(2df,2pd)
****
5 6 0
6-31+(2d,2p)
****
7 8 9 10 11 12 0
6-311++(2d,2p)
****
```

Figure 15.1. HOMO (24th orbital).
Z-H-S-N=N-S-H

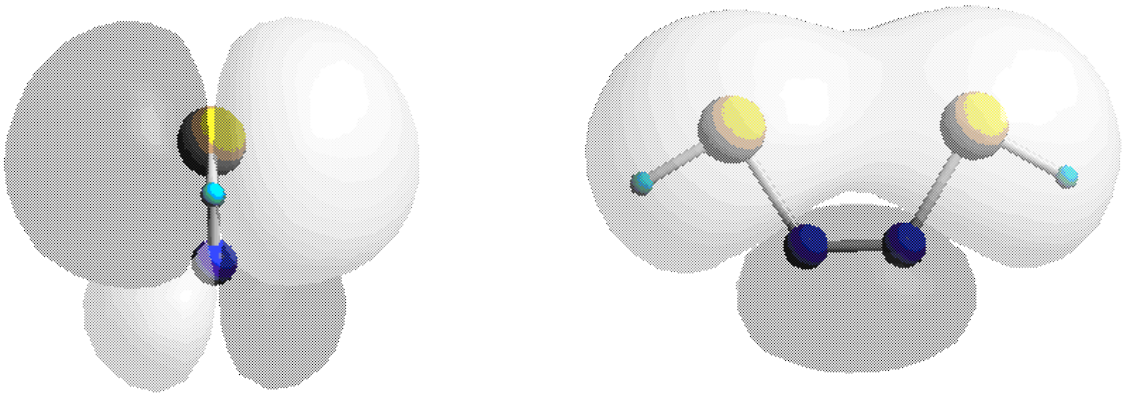

Figure 15.2. HOMO -1 (23th orbital).
Z-H-S-N=N-S-H

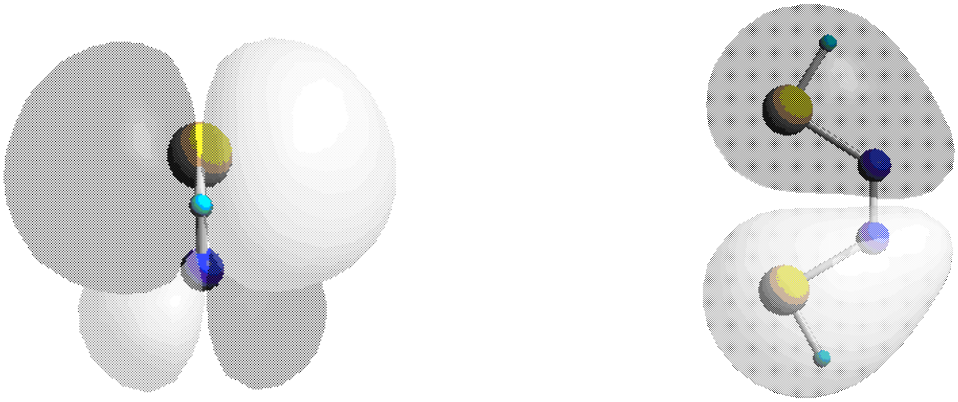

Figure 15.3. HOMO -2 (22th orbital).
Z-H-S-N=N-S-H

Figure 15.4. HOMO -3 (21th orbital).
Z-H-S-N=N-S-H

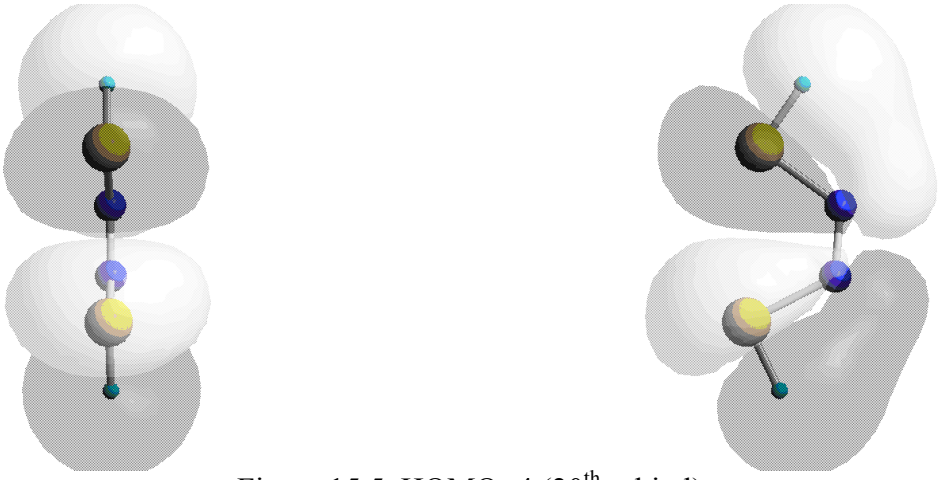

Figure 15.5. HOMO -4 (20th orbital).
Z-H-S-N=N-S-H

Figure 15.6. HOMO -5 (19th orbital).
Z-H-S-N=N-S-H

Figure 15.7. HOMO -6 (18th orbital).
Z-H-S-N=N-S-H

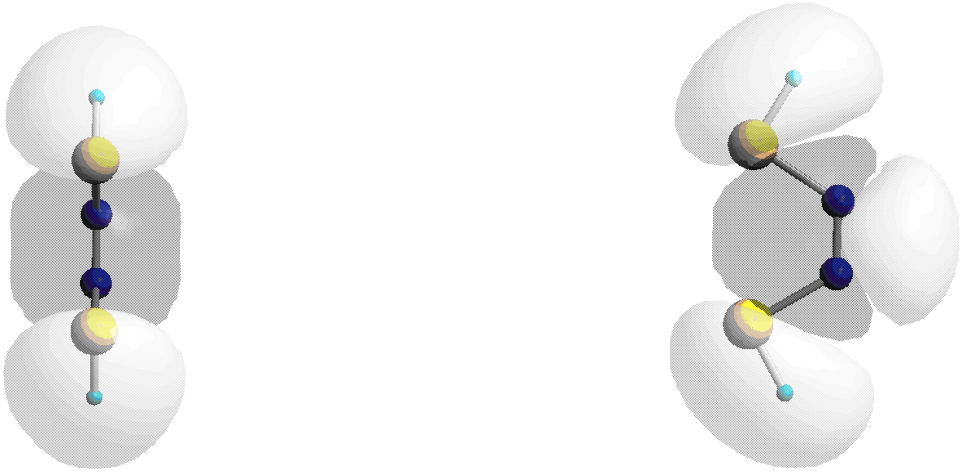

Figure 15.8. HOMO -7 (17th orbital).
Z-H-S-N=N-S-H

Figure 15.9. HOMO -8 (16th orbital).
Z-H-S-N=N-S-H

Figure 15.10. HOMO -9 (15th orbital).
Z-H-S-N=N-S-H

Figure 15.11. HOMO -10 (14th orbital).
Z-H-S-N=N-S-H

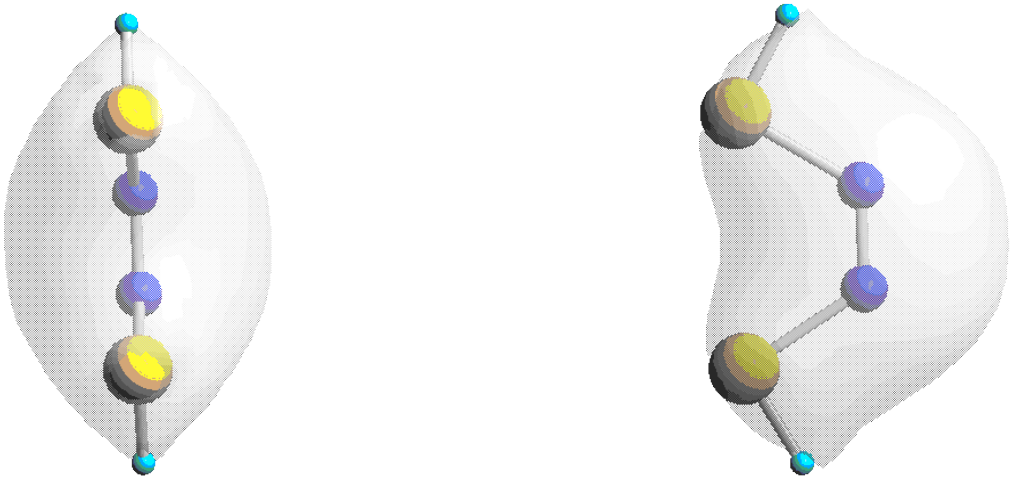

Figure 15.12. HOMO –11 (13th orbital).
Z-H-S-N=N-S-H